MEASUREMENT OF POINT VELOCITIES IN TURBULENT LIQUID FLOW

By

Ronald W. Greene and Stanley K. Burt

Research Report No. 83 December 1967

SPACE ENGINEERING
MISSISSIPPI STATE UNIVERSITY

SQ-51698

MEASUREMENT OF POINT VELOCITIES IN TURBULENT LIQUID FLOW

By Ronald W. Greene and Stanley K. Burt

Prepared under Contract No. NAS8-20383 by
Department of Aerophysics and Aerospace Engineering
Mississippi State University
State College, Mississippi

for

NATIONAL AERONAUTICS AND SPACE ADMINISTRATION

CONTENTS

MEASUREMENT OF POINT VELOCITIES IN TURBULENT LIQUID FLOW

By Ronald W. Greene and Stanley K. Burt

Department of Aerophysics and Aerospace Engineering
Mississippi State University

SUMMARY

The existing statistical theories of turbulence rely on data obtained experimentally for their implementation. Therefore, a method of determining statistical distributions of the necessary turbulence parameters is desired. The method was desired to be applicable to a system such as a liquid propulsion system; consequently, the investigation was carried out in the turbulent flow of water.

In general cases of nonsteady fluid motion, the hot-wire anemometer technique is a basic quantitative method for measuring velocity fluctuations. Extension of the hot-wire technique to conducting liquids by industry has produced changes in sensor design resulting in development of the quartz-coated, hot-film sensor. In Part I of this report, the hot-film technique is applied, as a basic experimental method, to the turbulent flow of water in a pipe. However, since the hot-film sensors are fragile and the associated equipment relatively complex, other methods of a simpler and more convenient nature are desirable. In Part II, an elementary photographic method is developed to obtain quantitative measurement of velocity fluctuations in the cases of turbulent flow behind a grid and in a pipe. The two methods are compared and evaluated.

INTRODUCTION

Turbulent flow is a random, fluctuating fluid motion and any device used to measure the characteristics of such motion must be able to respond to rapid fluctuations with negligible attenuation of the signal. This requires the measuring system to have a low inertia in order to respond rapidly. The measuring device must also be small enough to produce only minor interaction between itself and the surrounding fluid. The measuring device must also be stable enough so that the calibration will remain constant during at least one experimental run, and in the particular case of liquid flow, must be strong enough to exclude induced vibrations from the system.

Numerous methods have been proposed for measurement of turbulence in gases. However, the number of methods applicable to liquids is small. Four methods of note are the hot-wire or hot-film anemometer, electromagnetic induction, laser velocimeter, and flow visualization methods.

The most used method for the measurement of mean and fluctuational velocities in turbulent flow is the hot-wire or hot-film anemometer (Reference 19) which satisfies most of the requirements mentioned above. The use of hot-wire or hot-film anemometers has been much more limited in liquids than in air. One reason is that water, while being the liquid of most general interest, is also one of the most difficult liquids when making measurements with ordinary hot wires or hot films. Extension of the hot-wire technique to liquid flow has resulted in the development of the quartz-coated, hot-film sensor which greatly improves the performance and stability of the sensor over that obtained with a wire or uncoated hot film.

Insulation of the platinum film by the quartz prevents electrolysis and reduces the tendency for deposits to collect on the sensor. However, investigations (Reference 9) have indicated a tendency for the quartz coating to erode after several hours of use. The problem of erosion of the quartz coating causes concern since frequent calibration must be conducted to insure repeatable results. Also, bubble formation can result inducing oscillation in the anemometer output. In spite of its associated difficulties and inherent nonlinearities (Reference 15), the hot-film anemometer, with quartz-coated sensors, provides an effective means for obtaining quantitative measurements in turbulent liquids.

In Part I of this investigation, the quartz-coated, hot-film, cylindrical sensor was employed to measure the turbulence intensities and mean velocity profiles in the turbulent flow of water in a pipe. An extension of this technique, the analysis of the anemometer signal to obtain the distribution of the velocity about its mean value at various radial locations, was also performed.

The method of electromagnetic induction, introduced by Kolin (Reference 16), uses the Maxwell-Faraday law to determine velocities perpendicular to an electromagnetic field in a liquid that is slightly ionized. Electrodes with a known spacing may be introduced into the fluid and by measuring the potential developed can be related to velocity of the fluid. The general equation is

$$V = \mu/c \; HUS$$

where V is the potential, μ the relative magnetic permeability of the liquid, c is the speed of light, U is the perpendicular velocity, H is the electromagnetic field strength, and S is the electrode spacing.

The advantage of this method is that the potential is a linear function of the perpendicular velocity and does not depend on viscosity, density, or composition of the fluid (Reference 15).

There are two ways in which electromagnetic induction may be employed. Either the whole flow field can be exposed to an electromagnetic field, or a small electromagnet connected to a pair of electrodes may be entered into the fluid in question. This second technique is not useful for measuring turbulent quantities unless they are very large, but Grossman (Reference 13) has successfully used the first technique (Reference 14) for the determination of root-mean square turbulent velocity components.

Another advantage that this system offers is that there is no thermal lag in the measuring device and no compensation circuitry is required, as with the hot-wire anemometer. The main disadvantage is that small transient potentials are being measured, on the order of 10^{-5} volts, and these may be obscured by spurious potentials of large magnitude unless experimental precautions are taken (Reference 13).

An interesting new method, the laser velocimeter, has been used to determine point velocities in turbulent pipe flow. The laser velocimeter utilizes its beam of light, generated by a He-Ne gas laser, and the Doppler principle to measure velocity. This method seems to have considerable merit in that there is no interference with the fluid flow and the frequency response of the electrical system, developed by the investigators, Welch and Tomme (Reference 24), is believed to be better than previous methods.

In a recent study on pipe flow turbulence, Chuang and Cernak (Reference 7) have inferred by the use of measured electrokinetic potential fluctuations the distribution of turbulent intensities, shearing stress, and energy spectra. This method is based on the electrokinetic phenomenon which was first formulated by Helmholtz and has recently been extended to turbulent shear flow. Chuang and Cernak claim good agreement with the results obtained by Laufer (Reference 17) and Sandborn (Reference 21). However, since no absolute calibration technique for calibrating the probe is known, only the functional forms of the various turbulent intensities are obtained (Reference 7).

The method of flow visualization has been known for a long time to give a qualitative representation of an instantaneous state of water flows. While work done with trace particles has been reported for many years, the use of trace particles for quantitative work is comparatively new. Fage and Presten (Reference 10) used aluminum powder for a quantitative study of flow around scale models of streamlined bodies in a water tunnel, and Fage and Townsend (Reference 11) used an ultramicroscope to study the movement of fine dust particles in a pipe.

Emulsions have also been used by various experimenters to study turbulent flow. These emulsions, such as benzene and carbon tetrachloride, can be made to have the same density as water, thereby reducing any error caused by different fluid densities. Gaffyn and Underwood (Reference 12) and Van Driest (Reference 23) have used this method for measurement of velocity distributions and diffusion coefficients, respectively. However, if this method is used for measuring high intensity turbulence, the droplets must be made small enough so that secondary droplets will not be produced due to the breaking up of the primary droplets.

The use of polystyrene spheres as tracer particles for giving both a qualitative and quantitative flow pattern has recently been used. Wintering and Deterding (Reference 25) used polystyrene tracers to study gaseous systems such as combustion chambers and furnaces. By the use of the tracer particles in water, they were able to simulate gas flows. Allen and Yerman (Reference 5) also used neutral density beads to study flow patterns through a transparent, rectangular-shaped tube of Lucite. A more recent study has been undertaken by Brooks (Reference 6) to observe convection velocities by using neutral density polystyrene beads.

If the size of the tracer particles used in the flow is smaller than that of the smallest scale of turbulence, then the particles may be taken to give a true representation of the non-steady flow, provided that the density of the particles is approximately the same as that of the fluid.

The method of using tracer particles in water flow offers the advantage that the procedure for data acquisition is quite simple and expensive electronic equipment is not necessary. This method also allows observation of the whole flow field, and the interference produced in the flow by a probe is eliminated.

In Part II of this report, an attempt is made to develop an elementary photographic method into a technique for quantitative measurement of turbulent quantities of intensity and

scale in turbulent water flow. Some examples of measured results are given for the turbulent flow behind parallel bars, a grid, and the turbulent flow in a smooth pipe. Results of the photographic method obtained for flow behind the grid and in pipe flow are compared with those obtained with a hot-film anemometer.

PART I. APPLICATION OF THE HOT-FILM ANEMOMETER TO TURBULENT LIQUID FLOW

INSTRUMENTATION

Test Facility

The pipe flow facility is shown schematically in Figure 1. The pipe was made of polyvinylchloride, had a 4-inch inside diameter, was 50 feet long and 5 feet high. The polyvinylchloride material was chosen to eliminate corrosion of the inside walls due to any residual minerals in the water. The test section, 2 feet in length, was made of clear Plexiglas* to aid in positioning, orienting, and inspecting the probe in situ.

Distilled water was pumped through the pipe by a jet pump system driven by a constant speed AC motor. Alteration of the flow rate was performed by changing the pulley-diameter ratio. Mean flow rate, on which Reynolds number was based, was measured via a calibrated venturi located in the downstream end of the lower leg of the pipe. A standpipe was added to allow the air liberated from the water during operation to escape. The standpipe was kept covered to prevent dust from falling into the liquid and subsequent contamination of the water.

Hot-Film Anemometer System

The hot-film system, shown in Figures 2a and 2b with the recording and playback instrumentation, was composed of Thermo-Systems, Inc. heat flux constant temperature anemometers Models 1010 and 1030, random signal correlator Model 1015, a random signal rms voltmeter, and a DC vacuum tube voltmeter. Two types of probes were used in this investigation - a single sensor for axial velocity and turbulence measurements and an x-array oriented for measurement of axial and radial turbulence intensities. The sensors were standard design, cylindrical hot-films with quartz coatings for use in liquids. The probes were positioned in the radial direction by means of the screw-type vernier apparatus shown in Figures 3 and 4. Accurate location of the probe was affected within ±0.0025 inch or ±0.125 percent of the pipe radius.

*Reg. T.M., Rohn and Haas Company

Counting System

Due to the sensitivity of the water properties to changes in temperature, run times were kept as short as possible to insure constant calibration. Also, the amount of material deposited on the probe is quite naturally a function of run time. These two points necessitated recording the anemometer output in order to obtain uniform samples for the frequency distribution measurements. However, the recording level was limited by the recorder amplifiers requiring either attenuation of the signal or suppression of a portion of it before recording. The former method was unacceptable since attenuation placed the fluctuating component within the noise level of the recording amplifier. The latter method was used and involved only the suppression of enough of the DC level of the voltage to allow the time varying component to be recorded. A small analog computer was used to suppress the signal and provide variable gain capability; thus, a signal of relatively constant strength was recorded at all radial locations. A third method was also tried, that of recording only the time variant voltage and reading the mean voltage off the anemometer meter. However, this method was discarded because the meter time constant was too short to assure accurate readings of mean voltage, especially near the wall in regions of high relative turbulence.

During playback, the signal was added to a reference potential of opposite sign, thus suppressing the signal again. The resultant signal was then fed into an electronic counter whose triggering level was maintained constant. Consequently, the counting level could be adjusted merely by altering the reference potential.

Schematic diagrams of the recording and playback systems are shown in Figures 5 and 6.

CALIBRATION PROCEDURE

The calibration of the sensor is of the utmost importance in low velocity flows if accurate absolute velocity is desired. The fundamental form (Reference 1) of the heat transfer-velocity relationship for liquids is

$$N_u = 0.43 + 0.534\ (R_e)^{0.5}\ P_r^{0.31} \qquad (1)$$

for

$$1 < R_e < 4000 \qquad (2)$$

where the fluid properties are evaluated at the film temperature, and the Reynolds number is based on sensor diameter. However, this equation did not yield acceptable results when applied to the flow system under investigation. Therefore, a calibration of the sensor was conducted.

A more general form of the previous equation in terms of bridge voltage, velocity, and temperature is

$$\frac{E^2 R_s}{(R + R_{comp} + R_s)^2} = (A + BV^n)(T_s - T_e) \tag{3}$$

For purposes of calibration this may be written as

$$E^2 = A^1 + B^1 V^n \tag{4}$$

where A^1 and B^1 are now explicit functions of resistance and temperature.

The cooling velocity V is given as

$$V = \sqrt{(\bar{U} + u)^2 + v^2 + w^2} \tag{5}$$

Raising V to the power n and expanding in a series yields

$$V^n = \bar{U}^n \left(1 + n\frac{u}{\bar{U}} + O(u^2, v^2, w^2)\right) \tag{6}$$

for

$$u \ll \bar{U},\ v \ll \bar{U},\ w \ll \bar{U}$$

Now, in the mean value V^n becomes $\bar{U}^n$, so

$$\overline{E^2} = A^1 + B^1 \bar{U}^n \tag{7}$$

As indicated by equation (1), n can be taken as 0.5, thus

$$\overline{E^2} = A^1 + B^1\overline{U}^{0.5} \qquad (8)$$

Calibration was first attempted using a tow-cart arrangement in which the probe was mounted on a three-wheel cart (Figure 7) which was towed along a water-filled channel. A timing gate consisting of two photo-sensitive diodes actuated an electronic clock thus providing an elapsed time over a predetermined distance of from 1 to 2 inches. The output of the anemometer was recorded and a timing mark used to indicate the passage through the gate. The average of the output was then taken as that corresponding to the velocity calculated from distance and elapsed time measurements. In general, the elapsed times were short enough so that the average output could be considered to be the instantaneous value indicated by the timing mark. The data thus obtained was plotted as $\overline{E^2}$ versus $\overline{U}^{0.5}$ and the water temperature noted. The method of least squares was then used to fit a linear curve to the data. This method was repeated for all sensors used in axial velocity measurements and was initially thought to be adequate due to the closeness of fit of the linear curve to the data.

However, subsequent measurements in the pipe facility yielded velocities in excess by as much as 50 percent when compared to Pitot-static tube measurements and mean flow values obtained from a calibrated venturi. The discrepancies in the calibrated and measured velocities are attributed to the different natures of the flows over the sensor in the two situations. The flow in the channel was due only to the motion of the sensor and consequently did not exhibit the generally random motion found in the pipe. This could account for the heat transfer from the sensor in the calibration channel being less than that found in the pipe resulting in lower calibration voltages. If, indeed, this is the case, serious consideration must be paid to the problem of calibration, particularly at low velocities, and whenever feasible, calibration should be accomplished in situ. Therefore, the sensors were recalibrated based on velocities obtained from pressure measurements made at various radial locations in the pipe.

In spite of attempts to filter the water, prolonged use resulted in deposits of lint and other material collecting on the sensors lowering sensitivity and associated voltages. This was found to be particularly bothersome in tap water and, although much reduced, still annoying when distilled water was substituted as the working fluid. The only reliable method of removing these deposits was found to be brushing

the sensors with a soft camel's hair brush. Extreme care, however, must be taken in this process to avoid breaking the fragile sensor or damaging the thin quartz coating. The use of a stereo microscope is desirable for evaluation of the brushing procedure.

The calibration of single element sensors for turbulence intensity measurements requires nothing more than the calculation of zero velocity output, $\overline{E_0}^2$. A simple method for doing this is to measure the output at zero velocity. Although this neglects free convection effects (Reference 1), quite good accuracy is obtained, particularly at low overheat ratios. An alternate method is to make readings at known velocities and extrapolate to zero velocity.

If all that is desired is the ratio of the velocity at point 1 to that at point 2, then the same situation exists from

$$\frac{\overline{U}_1}{\overline{U}_2} = \left[\frac{(\overline{E_1}^2 - A^1)/B^1}{\overline{E_2}^2 - A^1 \quad B^1}\right]^2 = \left[\frac{\overline{E_1}^2 - \overline{E_0}^2}{\overline{E_2}^2 - \overline{E_0}^2}\right]^2 \qquad (9)$$

Thus, velocity profiles can be obtained by merely noting the outputs at zero velocity and the velocities at the points in question. Care should be exercised, however, since E_0 is a strong function of temperature at low velocities and can vary appreciably in liquids if run times are long and no method of cooling the liquid is employed.

The calibration of the x-array probe used in measuring two perpendicular velocity fluctuation components requires evaluation of the deviation of the velocity over a yawed cylinder from a cosine power function (Reference 1). Thus, with

$$U = V\,(\sin\beta)^{1/k} \qquad (10)$$

it follows that

$$k = \tfrac{1}{2} \log\left[\sin\beta_1/\sin\beta_2\right] / \log\left[\frac{\overline{E_1}^2 - \overline{E_0}^2}{\overline{E_2}^2 - \overline{E_0}^2}\right] \qquad (11)$$

This is accomplished by orienting the sensor at two different angles, β, with respect to the flow direction and noting the outputs. The flow velocity need not be known but must be constant in its mean value at the point of measurement. The k

for both sensors can, in general, be considered to be the same. However, in this investigation k was found to vary between 1.10 and 1.20; consequently, an average of 1.15 was used.

In order to prevent boiling of the water, all sensors were operated at a constant overheat ratio of 1.10 which yielded operating temperatures (dependent on liquid temperature) of approximately 160 degrees F.

TEST PROCEDURE AND DATA REDUCTION

Measurement of axial and radial turbulence intensity was conducted with the x-array probe, and Thermo-Systems anemometers, Models 1010 and 1030, random signal correlator Model 1015, and a Hewlett-Packard random signal rms voltmeter which had been modified by Thermo-Systems to provide a slow averaging time of 20 seconds. The outputs of the anemometer units were fed into the correlator which was adjusted to provide the sum and difference of the signals or merely the outputs themselves. These quantities were then presented to the rms voltmeter and the respective voltages read on a vacuum-tube voltmeter connected to the output of the rms meter. This was necessary since the rms meter only represented the value of the fast (2-second) averaging time and was not designed to indicate the slow averaging time. Mean voltages were measured on a digital voltmeter with the correlator in the DC mode. The data thus obtained was substituted into the following equations (Reference 1) which yielded the desired turbulence levels and correlation coefficients at various radial locations.

Axial turbulence intensity

$$\frac{\sqrt{\overline{u^2}}}{U} = \frac{1}{n}\left[\frac{\left(\sqrt{\overline{e_I^2}}\right)^2 \overline{E_I^2}}{\left(\overline{E_I^2} - \overline{E_{I_o}^2}\right)^2} + \frac{\left(\sqrt{\overline{e_{II}^2}}\right)^2 \overline{E_{II}^2}}{\left(\overline{E_{II}^2} - \overline{E_{II_o}^2}\right)^2} + \frac{\left(\sqrt{\overline{(e_I + e_{II})^2}}\right)^2 - \left(\sqrt{\overline{(e_I - e_{II})^2}}\right)^2}{\left[\left(\overline{E_I^2} - \overline{E_{I_o}^2}\right)\left(\overline{E_{II}^2} - \overline{E_{II_o}^2}\right)\right] / \overline{E_I}\ \overline{E_{II}}}\right]^{\frac{1}{2}} \quad (12)$$

Radial turbulence intensity

$$\frac{\sqrt{\overline{v^2}}}{\overline{U}} = \frac{k\ \tan\beta}{n}\left[\frac{(\sqrt{\overline{e_I^2}})^2\ \overline{E_I}^2}{(\overline{E_I^2} - \overline{E_{I_o}^2})^2} + \frac{(\sqrt{\overline{e_{II}^2}})^2\ \overline{E_{II}}^2}{(\overline{E_{II}^2} - \overline{E_{II_o}^2})^2} - \frac{1}{2}\ \frac{\left(\sqrt{\overline{(e_I + e_{II})^2}}\right)^2 - \left(\sqrt{\overline{(e_I - e_{II})^2}}\right)^2}{\left[(\overline{E_I^2} - \overline{E_{I_o}^2})(\overline{E_{II}^2} - \overline{E_{II_o}^2})\right]/\overline{E}_I\ \overline{E}_{II}}\right]^{\frac{1}{2}} \quad (13)$$

The uv correlation coefficient is given by

$$R_{uv} = \frac{\overline{uv}}{\sqrt{\overline{u^2}}\ \sqrt{\overline{v^2}}} = \left\{\frac{k\ \tan\beta}{n^2(\sqrt{\overline{u^2}}/U)(\sqrt{\overline{v^2}}/U)}\right.$$
$$\left.\left[\frac{(\sqrt{\overline{e_I^2}})^2\ \overline{E_I}^2}{(\overline{E_I^2} - \overline{E_{I_o}^2})^2} - \frac{(\sqrt{\overline{e_{II}^2}})^2\ \overline{E_{II}}^2}{(\overline{E_{II}^2} - \overline{E_{II_o}^2})^2}\right]\right\} \quad (14)$$

Mean velocities were measured at various radial locations by reading the mean output and applying the calibration curve obtained for the particular sensor.

The single sensor was used in the analysis of the distribution of the axial velocity about its mean value. The voltage from the anemometer was fed into the analog computer where a constant voltage of opposite sign was added to it. The resultant signal was amplified or attenuated, dependent on its magnitude, in order that the fluctuating component plus a small DC component would be recorded. This signal was kept in the range of 0.5 to 1.0 v to comply with recorder limits, and the amount of suppression voltage and attenuation or gain was noted. This procedure was repeated at each radial station investigated for a constant recording period of 25 sec/station.

Several runs at two different Reynolds numbers were taken with one traversal of the pipe radius constituting a run. However, the data thus obtained exhibited no definite variation with

Reynolds number so the results of only one Reynolds number (1.2×10^5) are presented in this report.

The voltages recorded were analyzed using the counting system described previously. The distribution of the voltages was analyzed to find the mean square, and from this, the mean velocity was determined. The fluctuating component represented by each voltage level was determined from

$$E^2 = E_o^2 + B'\bar{U}^n \left(1 + n\frac{u}{\bar{U}}\right) \tag{15}$$

and since

$$\overline{E^2} = \overline{E_o^2} + B'\bar{U}^n \tag{16}$$

then, with $n = 0.5$

$$\frac{u}{\bar{U}} = 2\left(\frac{E^2 - \overline{E^2}}{\overline{E^2} - \overline{E_o^2}}\right) \tag{17}$$

Thus, the ratio of the instantaneous velocity at a point to the mean velocity may be given as

$$\frac{\bar{U} + u}{\bar{U}} = 1 + \frac{u}{\bar{U}} = 1 + 2\left(\frac{E^2 - \overline{E^2}}{\overline{E^2} - \overline{E_o^2}}\right) \tag{18}$$

Of course, this neglects terms of the order $u^2/\bar{U}^2$ and above as well as the effect of the other two velocity components. However, for a small turbulence level, this is not of major concern.

The frequency distributions of the velocity ratio were then integrated and the frequency ordinate adjusted to satisfy the requirement that the area under the curve be unity. The trapezoidal rule was used in all moment and area calculations.

The variance of the velocity ratio about its mean was determined from the second moment of the area about the mean. The square root of the variance is the standard deviation and represents the rms of the fluctuating component and as such, is the turbulence intensity. The turbulence intensities

obtained in this manner were compared with those obtained by the procedure of Reference 1 and are presented in other portions of this report.

Although not attempted, the distribution of the radial and tangential components about their mean values of zero could be obtained by using an x-array probe and recording the outputs of both wires simultaneously. However, difficulties encountered in attempting to keep the sensors free of dirt or lint particles makes the problem of maintaining two sensors clean simultaneously quite demanding. The assumption of uniform contamination of both sensors seems questionable, particularly at low velocities when the relative change in voltage can be great. This would definitely require recording the anemometer outputs and short run times to insure constant calibration of both sensors. Considering the equations for the x-array probe (Reference 1) before taking the rms values yields

$$\frac{2E_I(E_I - \overline{E_I})/n}{\overline{E_I^2} - E_{I_o}^2} = \frac{u}{U} + \frac{1}{k}(\cot\beta)\frac{v}{U} \tag{19}$$

for the sensor positively inclined (sensor I) with respect to the flow and

$$\frac{2E_{II}(E_{II} - \overline{E}_{II})/n}{\overline{E_{II}^2} - E_{II_o}^2} = \frac{u}{U} - \frac{1}{k}(\cot\beta)\frac{v}{U} \tag{20}$$

for a negatively inclined sensor (II). Summing the two equations yields

$$\frac{u}{U} = \frac{1}{n}\left[\frac{E_I(E_I - \overline{E}_I)}{\overline{E_I^2} - E_{I_o}^2} + \frac{E_{II}(E_{II} - \overline{E}_{II})}{\overline{E_{II}^2} - E_{II_o}^2}\right] \tag{21}$$

The difference in the two equations yields

$$\frac{v}{U} = \frac{k \tan\beta}{n} \left[\frac{E_I(E_I - \overline{E}_I)}{\overline{E_I^2} - E_{I_o}^2} - \frac{E_{II}(E_{II} - \overline{E}_{II})}{\overline{E_{II}^2} - E_{II_o}^2} \right] \qquad (22)$$

In order to use the counting method, the voltage E_I and E_{II} must be recorded in the manner mentioned previously. Then each signal should be analyzed individually to obtain the mean values needed in Equations (21) and (22). Using these values as constants, the analog computer can be used to synthesize the function given in Equations (21) and (22) which can then be counted by the techniques of this investigation. A similar procedure can be used to obtain joint probability distributions for two different locations or two different velocity components.

PRESENTATION OF RESULTS

The measurements made in turbulent pipe flow with the hot-film anemometer consisted of mean velocity, axial, and radial turbulence intensity, uv-correlation coefficient, and distribution of the instantaneous axial point velocity about its mean for various Reynolds numbers ranging from 10^4 to 10^5. No significant variation with Reynolds number could be inferred from this restricted range; therefore, the results of only one, $R_e = 1.2 \times 10^5$, are presented.

The mean velocity profile, typical of those obtained at the test R_e, shown in Figure 8, was obtained from the mean velocities computed by the counting method and compares favorably with the 1/7 power law (Reference 22).

The axial turbulence was measured in three ways. The first procedure was to use an x-array and obtain both axial and radial intensities. The axial intensity was also measured using a single sensor normal to the flow. Measurements with the x-array and single sensor were accomplished using the standard procedure of Reference 1. The results of these measurements are shown in Figure 9. Shown in the same figure is the axial turbulence intensity as obtained with the single sensor by the counting procedure associated with the velocity occurrence distributions. The standard deviation of such a distribution is essentially the rms value of the fluctuating component and as such, is the same as the turbulence intensity. The turbulence intensities obtained by both methods with the

single sensor agree favorably with each other, but fall below those obtained using the x-array probe. Also, the values measured with the x-array fall below the results obtained by Laufer and Sandborn in air (References 17 and 21). The discrepancy between the x-array and single sensor measurements is perplexing since, in most instances, the single sensor is used to check the performance of the x-array. The single-sensor probe was used more extensively than the x-array which could have resulted in aging and reduction of sensitivity. Inspection of the sensor under a stereo microscope did disclose deposits of foreign material. In an effort to dislodge these deposits, a soft camel's hair brush was used. Although the brushing procedure was moderately successful, its effect on the thin quartz coating is not known. However, one sensor used which had not been subjected to the brushing procedure was noticed to form bubbles due to a portion of the quartz flaking off. No bubbles were noticed on the probes subjected to brushing. Regardless of the discrepancy between x-array and single sensor results, the agreement of the counting method and standard method for determination of turbulence intensity with the single sensor provides ample verification of the counting technique for turbulence measurements.

The radial turbulence intensity and cross correlation coefficient, R_{uv}, shown in Figures 10 and 11 also fall below the data of Laufer and Sandborn, but again, the trend is the same for both cases.

The disagreement of the results of this investigation with those obtained by others in air is not unexpected. In fact, comparison of two different pipe facilities in the same fluid medium is difficult if not questionable. Couple this difficulty with the added problem of different fluids and any comparison must be restricted to qualitative analysis alone.

The distribution of axial velocity about its mean value is shown in Figures 12a, 12b, 12c, 12d, 12e, and 12f for six radial locations. In these figures, the distributions obtained by the counting method are compared with the normal Gaussian curve as computed for the measured standard deviation at the radial location indicated. The results agree favorably with the Gaussian function indicating that the distribution is approximately normal. This, although expected near the center line, is not necessarily the expected result near the wall. Results of Welch and Tomme (Reference 24) indicate a skewness in the distribution as the wall is approached. Deviation from the normal distribution for the data in this investigation is more pronounced near the wall, but no definite skewness variation with radial location can be inferred. Attempts were made to obtain quantitative measurements of skewness and

flatness from the distributions by computing the third and fourth moments of the area about the mean. However, due to the sensitivity of higher order moments such as these to small deviations at large distances from the mean, no reliable quantitative results were obtained. Nevertheless, varying degrees of skewness were evident with the skewness increasing from near zero at the pipe center to positive values near the wall. The presence of the wall was also felt in the flatness measurements which qualitatively exhibited increasing flatness with decreasing distance from the wall. The measurements of skewness and flatness could undoubtedly be improved if more counting levels were utilized, particularly on the tails of the curves.

In an effort to display the distributions on the radius for comparison, they are plotted in Figure 13. Each distribution is located on the radius by its mean value. That is, the distribution measured at $Y/R_p = 0.500$ has its mean value located at $Y/R_p = 0.500$ on the abscissa. The abscissa scale has no bearing on the shapes of the curves; however, all curves are based on identical horizontal and vertical scales. The solid lines are drawn through the data points and are not the computed Gaussian distributions. From this figure it is obvious that the relative turbulence varies as indicated in Figure 9 since the distributions widen as the wall is approached.

PART II. APPLICATION OF PHOTOGRAPHIC TECHNIQUE TO QUANTITATIVE MEASUREMENT OF VELOCITY FLUCTUATIONS IN TURBULENT LIQUID FLOW

PRINCIPLE OF MEASUREMENT

If small, insoluble particles are introduced into fluid flow, their paths can be recorded by motion picture or by short-duration, flash photographs. Particles which have the same density as the fluid under observation are not affected by gravity, and if the dimensions of the particles are very small, the effect of an interaction with the surrounding fluid is small. Therefore, they can be taken to trace out patterns almost identical with the actual flow. This is a prime factor in evaluating the usefulness of the discrete particle method.

By short-duration, flash photographs with known exposure times, it is possible to evaluate the displacement of the particles according to both the magnitude and direction. If a fast shutter speed is used, the locus of tracer particles will be

approximately that of a fluid particle moved by the instantaneous velocity. When the main flow is parallel to the photographic plane, the mean velocity, as well as the lateral and vertical fluctuating velocity components in this plane, can be determined.

The paths of the particles are recorded on the film with a known shutter speed. The length of the particle trace and the angle that the trace makes with the reference direction is recorded. The magnitude of the particle's streak is then broken up into its parallel and perpendicular components to the reference direction and from this data the two components of velocity fluctuation can be calculated.

As shown in Figure 14, the x-axis is taken to be parallel to the mean velocity. When the vector $\overline{OA}$ represents an instantaneous velocity vector and $\overline{OB}$ and $\overline{OC}$ are the orthogonal trajectories to the xy- and xz-planes, respectively, then the velocity components are

$$U = OB\cos\theta, \qquad V = OB\sin\theta, \qquad W = OC\sin\phi$$

When the photographic plane of the camera is made parallel to the xy-plane, the length of OB and the angle θ can be seen in every photograph for the total number of N. Then, the mean velocity $\overline{U}$ and components of turbulent intensity in the xy-plane can be evaluated as follows:

$$\overline{U} = \lim_{N\to\infty} \frac{1}{N} \sum_{i=1}^{N} a_i\cos\theta_i$$

$$\overline{u^2} = \lim_{N\to\infty} \frac{1}{N} \sum_{i=1}^{N} (a_i\cos\theta_i - \overline{U})^2$$

$$\overline{v^2} = \lim_{N\to\infty} \frac{1}{N} \sum_{i=1}^{N} (a_i\sin\theta_i - \overline{V})^2$$

$$\overline{uv} = \lim_{N\to\infty} \frac{1}{N} \sum_{i=1}^{N} (a_i\cos\theta_i - \overline{U})(a_i\sin\theta_i - \overline{V})$$

Where a_i is the length of the particle trace and θ_i is the angle that a_i makes with the reference direction. Other components multiplied by w can also be derived by taking

photographs at the same time with another camera whose photographic plane is made parallel to the xz-plane.

Euler correlations at two points are also evaluated by the same procedure. Namely, velocity components can be decided from each picture at two points in the flow, and the mean values of correlations are evaluated as

$$\overline{uu_1} = \lim_{N\to\infty} \frac{1}{N} \sum_{i=1}^{N} (a_i \cos\theta_i - \overline{U})(a_i \cos\theta_{1i} - \overline{U}_1)$$

If N_u is the number of data in the total number N whose values are between U and U + ΔU,

$$\frac{N_U}{N}$$

is taken as the probability of the occurrence of a velocity between U and U + ΔU, and the frequency distribution function of U is easily calculated from the data. These analyses can be easily made by means of digital computer techniques.

EXPERIMENTAL PROCEDURES OF PHOTOGRAPHIC METHODS

Two series of experiments were performed. The first measurements were taken in a small-scale water tunnel with a 4-inch by 4-inch by 20-inch Plexiglas test section. In this small tunnel, shear turbulence was produced by the use of six stainless steel cylinders, and isotropic turbulence was produced by a grid of steel bars. It was felt that, particularly in the case of isotropic flow, the value of the photographic method could be ascertained by comparing the results with those predicted by theory.

The final experiment was performed in the polyvinylchloride pipe mentioned in Part I of this report. By performing these tests, the photographic method could be compared directly with the hot-film anemometer.

Experiment 1. - Two cases were studied in the small-scale water tunnel. They were two-dimensional, homogeneous turbulence and three-dimensional, homogeneous, isotropic turbulence. In both cases, in order to keep the flow uniform and to prevent the formation of air bubbles in the test section, a 4-inch by 4-inch by 2-inch aluminum honeycomb was installed in the throat entrance of the test section. For the production of homogeneous turbulence, six stainless steel cylinders, 4 in. long and 0.25 in. in diameter were mounted parallel

in the test section. Figure 15 shows the experimental arrangement used for the tests. Similarly, for the generation of a homogeneous and isotropic turbulence, a grid, consisting of steel bars 0.125 $in.^2$ with 0.5 in. mesh lengths was mounted at the same position of the test section. To prevent rust, the grid was painted with a thin coat of aluminum paint. The velocity of the flow was adjusted by means of a disc valve until the velocity was at its maximum value just before large air bubbles were introduced into the test section and completely disruptive cascade flow occurred.

The tracer particles introduced into the flow in order to make the flow path visible were spherical, polystyrene beads which had been sprayed with fluorescent red paint to give a high contrast with the black background used for photographic purposes. Before the beads were painted, approximately 80 percent of the particles had the same density as the water while the other 20 percent were slightly heavier. The difference in density gave a velocity, due to gravity, of 0.25 in./sec. After being sprayed, the density of the particles increased and the gravitational velocity increased to approximately 0.40 in./sec with a few particles having the same density as water. It was felt that this difference was small enough when compared to the mean velocities in the parallel bars and grid cases of 13.24 in. sec and 15.24 in. sec, respectively, to give a good representation of the fluid flow pattern.

Since the small-scale water tunnel was constructed so that some parts of it were open to the atmosphere, it was not necessary to have a special device to introduce the polystyrene spheres into the water flow. These particles could be added by hand and the concentration of the particles changed by filtering some particles out. It was found that in order for the polystyrene spheres to become involved in the water flow, they should be mixed with water in a separate container and then injected into the flow; otherwise, surface tension caused the particles to float on the surface until the particles were thoroughly wetted.

A 35mm Nikon camera, operating at a shutter speed of 1/30 sec, was mounted directly in front of the test section to record the particle traces on film. The camera has an electric motor-drive which, when connected to an auxiliary power supply, will take pictures at the rate of 3 frames per sec. This facilitated the taking of the photographs and lessened the possibility of disturbing the position of the camera.

The camera was shielded from glare and reflections by means of black cardboard, which completely eliminated these two disadvantages. It is absolutely necessary that proper illumination

be obtained. Since the polystyrene beads were distributed continuously throughout the flow field, two narrow slits, 0.25 in. wide and 20 in. long, were mounted on both sides of the test section to make the particles visible in a plane. To further isolate the particles, the camera was equipped with an extension tube and adjusted until the combination of shutter speed and f number gave a depth of field of 0.0625 in. on either side of the center of the plane of measurement. The position and width of the slit decide the position and area of measuring along the Z-axis.

Experiment 2. - The second series of measurements were carried out in the polyvinylchloride pipe. These measurements were made at a Reynolds number of 1.24×10^5. Red fluorescent beads of the same type as those used in the small-scale water tunnel tests were used in this series of experiments. Since the Plexiglas test section was curved, a Plexiglas box was built around the test section and filled with water in order to lessen the appearance of curvatures on the film resulting from the distortion of the light beam. A narrow slit was again used to provide illumination and the camera, operating at a shutter speed of 1/125 sec, was sheltered from all glare.

Instead of selecting one position at which to measure the turbulent quantities, as in the previous case, several different positions were taken along the radius of the pipe and the mean velocity and velocity fluctuations were obtained at these points.

PRESENTATION OF RESULTS OF PHOTOGRAPHIC METHOD

By the method employed in this investigation, values of $\overline{U}$, $\sqrt{\overline{u^2}}$, $\sqrt{\overline{v^2}}$, $\overline{uv}$, and the probability distribution of an instantaneous velocity U, were measured at a position, downstream from the parallel bars or grid, where the state of turbulence seemed to be homogeneous. The data were taken in the center positions of the test section having a small volume of $(0.25 \text{ in.})^3$ at positions 5.48 in. and 6.35 in. downstream from the parallel bars and grid, respectively. The shutter speed used in recording the particle tracer was 1/30 sec.

Mean velocities in the cases of parallel bars and grid were 13.24 in./sec and 15.25 in./sec, respectively. In the case of parallel bars, the values of $\sqrt{\overline{u^2}}$, $\sqrt{\overline{v^2}}$, and $\overline{uv}$ were 2.79 in./sec, 1.27 in./sec and 0.0282 $\text{in.}^2/\text{sec}^2$, respectively, and in the case of grid, they were 1.68 in./sec, 0.94 in./sec, and 0.00897 $\text{in.}^2/\text{sec}^2$. These numberical results indicate that at the positions of measurement, the situation of flow may not yet have attained that of an ideally homogeneous and isotropic turbulence, even in

the case of the three-dimensional grid. The frequency distributions of U are plotted for the two cases in Figures 16 and 17. In the case of the grid, the frequency distribution gives an almost symmetrical Gaussian distribution function.

In these measurements, it is desirable to determine the number of photographs which must be made to insure that a statistically-correct sample was taken. The plots of several mean values and $\sqrt{\overline{u^2}}$, $\sqrt{\overline{v^2}}$, and $\overline{uv}$ against the total number of N for the two cases are shown in Figures 18 and 19. It is seen that about two hundred data points are sufficient in both cases to give a good representation of the mean values.

A comparison of measurement was made by the photographic and hot-wire methods with an x-array in the case of grid flow. The values of $\overline{u^2}/\overline{U}$, $\overline{v^2}/\overline{u}$, and U (in./sec) by the photographic method were 0.11, 0.062, and 15.2 in./sec, respectively, and by the hot-film method they were 0.23, 0.25, and 16.0, respectively. Frequency distribution by the two methods is given in Figure 20.

One source of dissimilarity in the results may be the formation of microscopic air bubbles on the hot film. These small bubbles were inherent in the apparatus being used due to the process of aeration caused by the pumping motion of the circulating pump. These attached bubbles were seen to cause a drop in mean voltage and to induce an oscillation in the fluctuating component. This oscillation coupled with the drop in mean voltage is believed to be the reason for the higher turbulence levels measured by the hot-film method.

Using the photographic method, the values of $\overline{U}$, $\sqrt{\overline{u^2}}/\overline{U}$, $\sqrt{\overline{v^2}}/\overline{U}$, and the frequency distribution were calculated at seven different radial pipe locations and the results are shown in Figures 21 through 23. A plot of the correlation coefficient, R_{uv} is given in Figure 11.

The value of $\overline{U}/\overline{U}_{max}$, when compared to the 1/7 power law curve and to the data obtained by use of the hot-wire anemometer exhibited good agreement. However, the values of turbulent intensities differed significantly with those obtained by the hot-wire results. The measurements were also higher than those obtained by Laufer and Sandborn (References 17 and 21) using the hot-wire method and air as the medium. These results can be seen in Figures 21 and 22.

From the experiments in the miniature water tunnel, it was thought that 150 data points at each location should be sufficient for determining the turbulent quantities in the pipe. Since, in both cases measured in the small tunnel, the values

of $\bar{u}$, $\sqrt{\overline{u^2}}$, $\sqrt{\overline{v^2}}$, and $\overline{uv}$ were fairly stabilized after 150 data points. It is shown in Figure 21 that when 150 points are taken at one location and 300 pictures are taken at the same location, the value of u-intensity varies, but the results are still higher than those obtained by other experimenters.

The frequency distributions were plotted by normalizing the function and using the u-intensity as the standard deviation for calculating the Gaussian distribution. The frequency distributions obtained by the photographic method were broader than those obtained by the hot-wire. This indicates that the method displays an apparent sensitivity to only large-scale turbulent fluctuations and obscures the higher frequency and smaller amplitude fluctuations. However, the extent to which the method ignores the smaller scale turbulence is not known at present.

It was found that the frequency distribution based on the photographic method was far more sensitive to the number of photographs taken than was the turbulence intensity. Although the intensity measurements were fairly stable after 300 data points, not enough points were taken to give a true representation of the frequency distribution and the points were too scattered to allow a curve to be drawn through them. A representative graph of this erratic frequency occurrence is shown in Figures 23a and 23b.

The correlation coefficient, when measured by the use of tracer particles, was lower than when obtained by the hot-wire film. This is most probably due to an inertial lag in the bead response and was expected. A comparison of the shearing stresses obtained by both methods is given in Figure 11.

The main advantage of the tracer particle method is the essential promise of simplicity or convenience. If the particles used are strictly of neutral density and are smaller than the smallest scale of turbulence, then the particles should trace out the actual flow pattern. However, even though the analysis of data can be made rapid by the use of high-speed, digital computers, the reading of the film is tedious and laborious. Even though only 200 data points will determine the mean velocities, the frequency distribution results indicate that at least 500 data points are needed to accurately determine the intensities and possibly twice that for the frequency distribution curves.

The main source of error is in the reading of the particle trace. This error can be as large as 10 percent if the images of the tracer particles are not clear. Since the intensity is a function of $(U - \overline{U})^2$, any large variation is magnified, thereby causing higher readings of intensity. Also, inherent in the method is the assumption that the velocity is constant over the exposure time. Consequently, the higher frequency fluctuations, whose periods are less than the exposure time, will be averaged out resulting in measurements of only the lower frequency, larger amplitude fluctuations. The result is a turbulence intensity of larger magnitude due to the lack of sensitivity to the smaller fluctuations.

Decreasing the exposure time would improve the frequency sensitivity of the method. However, one must not shorten the trace to the extent that the error due to reading the film is comparable to the increased sensitivity.

Another difficulty experienced which could lead to experimental errors was the fact that the light reaching the camera passed through three different mediums. The error due to this refraction was not taken into account, although an attempt was made to lessen the appearance of curvature by installing a water-filled, Plexiglas box around the circular test section. There appeared to be no change in the curvature in these photographs compared to those in the small-scale water tunnel, but the photographs were not as sharp and were therefore more difficult to read.

Although this method gave different results than those obtained by the hot-wire, this does not detract from the method at this point. By using better lighting arrangements and a faster shutter speed, the numerical results obtained should be better. The higher intensities recorded also indicate that study should be conducted on bead or particle response in an effort to determine its effect on turbulence intensity measurements.

CONCLUSIONS

The application of hot-film anemometry to the turbulence of liquids is practical if adequate precautions are taken to ensure that a minimum of impurity is present. The calibration of the equipment is not overly demanding; however, one must be prepared to recalibrate quite often and in the test environment, if possible.

The counting method used, though rudimentary, appears adequate. However, the time required to analyze the signal at several different radial locations indicates a need for multi-channel capability, i.e., multiple counting levels. This would entail reading the outputs of several different counting circuits simultaneously which could be done photographically or digitally. The counting method, with some modification, can be extended to consider the joint probability distributions necessary for complete analysis of turbulent motion through the use of multi-sensor probes and additional recording circuits.

The frequency distributions of the axial velocity obtained with the counting method indicate relatively little deviation from the normal distribution with the exception of the wall region. Further investigation in this region is warranted with obtaining quantitative skewness and flatness variations as a primary goal.

The photographic method is shown to be an effective technique for measuring mean velocities in liquids. However, the turbulence levels or intensities measured are, in general, higher than those obtained by the hot-film method. Such disagreement may be attributed, at least in part, to the assumption that the velocity is constant during the exposure period which neglects higher frequency and smaller amplitude fluctuations. Also, the effect of the inertia of the bead on its response to higher frequency fluctuations is not known. It is felt that the photographic method can most effectively be applied to flows of high turbulence in which the hot-film method is seriously hampered by its inherent nonlinearities.

APPENDIX

SYMBOLS

A,B	hot-film calibration constants
a_i	length of particle trace, inch
c	velocity of light, meter/second
E	bridge output voltage, volts
e	bridge voltage fluctuation, volts
F	induced electric field strength, volt/meter
H	electromagnetic field strength, ampere-turn/meter
k	x-array calibration constant, nondimensional
N	number of data points taken
N_u	Nusselt number, nondimensional
n	exponent relating fluid velocity to heat transfer from sensor, nondimensional
P_r	Prandtl number
R	resistance of bridge leg in series with sensor, ohms
R_{comp}	resistance of probe and cable, ohms
R_e	Reynolds number
R_p	pipe radius, feet
R_s	sensor resistance, ohms
R_{uv}	uv-correlation coefficient $\frac{\overline{uv}}{\sqrt{\overline{u^2}}\sqrt{\overline{v^2}}}$
s	distance between electrodes, meters
T	temperature, °R
U	axial velocity, feet/second
$\overline{U}$	mean axial velocity, feet/second
U_p	velocity perpendicular to electromagnetic field, meter/second

$\frac{\sqrt{\overline{u^2}}}{\overline{U}}, \frac{\sqrt{\overline{v^2}}}{\overline{U}}, \frac{\sqrt{\overline{w^2}}}{\overline{U}}$	turbulence intensities in each of the cylindrical coordinate directions, non-dimensional
u, v, w	velocity fluctuation components in cylindrical coordinates, feet/second
V	fluid velocity, feet/second
y	distance from pipe wall, feet
β	angle at which sensor is inclined with respect to flow velocity vector, degrees
μ	relative magnetic permeability, newtons/ampere^2
θ	angle that particle trace makes with reference line, degrees

Subscripts

e	fluid conditions
s	sensor conditions
o	zero flow conditions
I	sensor 1
II	sensor 2

REFERENCES

1. ____, APPLICATIONS OF THE HEAT FLUX SYSTEM IN LOW TEMPERATURE GASES AND LIQUIDS, Technical Bulletin No. 4, Thermo-Systems, Inc., Minneapolis, Minnesota.

2. ____, DISA Electronics, COATED HOT FILM PROBES FOR MEASUREMENT IN LIQUID, DISA Information-Electronic Measurements of Mechanical Events, No. 3.

3. ____, HEAT FLUX SYSTEM, Model 1010, Instruction Manual, Thermo-Systems, Inc., Minneapolis, Minnesota.

4. ____, PRELIMINARY INSTRUCTION MANUAL, Model 1015 Correlator, Thermo-Systems, Inc., Minneapolis, Minnesota.

5. Allen, Merton and Yerman, A. J., NEUTRAL BEADS FOR FLOW VISUALIZATION, ASME Symposium on Flow Visualization, 1960.

6. Brooks, Richard Van, FREE CONVECTION VELOCITY MEASUREMENTS BY THE USE OF NEUTRAL DENSITY PARTICLES, Master's Thesis, Georgia Institute of Technology, Atlanta, Georgia, 1965.

7. Chuang, Hsing and Cernak, J. E., AICME Journal, 13,266, March, 1967.

8. Corrsin, S., TURBULENCE: EXPERIMENTAL METHODS: Handbuch Der Physik, Vol. VIII/2, Fluid Dynamics II, Berlin, Germany, 1963.

9. Delleur, J. W., Toebes, G. H., and Liu, C. L., HOT WIRE PHYSICS AND TURBULENCE MEASUREMENTS IN LIQUID, Technical Report No. 13, Hydromechanics Laboratory, School of Civil Engineering, Purdue University, Lafayette, Indiana, February, 1966.

10. Fage, A. and Presten, J. H., Journal of the Royal Aeronautical Society, 45,124, 1941.

11. Fage, A. and Townsend, H. C. H., Proclamation of the Royal Society of London, 135A 656, 1932.

12. Gaffyn, J. E. and Underwood, R. M., NATURE, 169,239, 1952.

13. Grossman, L. M. and Shay, E. A., MECHANICAL ENGINEERING, 71,744, 1949.

14. Grossman, L. M. and Charwatt, A. F., Rev. Sci. Instr. 23,741, 1952.

15. Hinze, J. O., TURBULENCE, McGraw-Hill Book Publishing Company, Inc., New, New York, 1959.

16. Kolin, A., PROCLAMATION OF THE SOCIETY OF EXPERIMENTAL BIOLOGICAL MEDICINE, 35,53, 1936.

17. Laufer, John, THE STRUCTURE OF TURBULENCE IN FULLY-DEVELOPED PIPE FLOW, NACA TN 2954, June 1953.

18. Lin, C. C., TURBULENT FLOW: THEORETICAL ASPECTS, Handbuch Der Physik, Vol. VIII/2, Fluid Dynamics III, Berlin, Germany, 1963.

19. Ling, S. C. and Hubbard, P. T., Journal of Aeronautical Society, 23,890, 1956.

20. Macovsky, Morris S., THE MEASUREMENT OF TURBULENCE IN WATER, Report No. 670, Navy Department, The David Taylor Model Basin, Washington, D. C., October, 1948.

21. Sandborn, Virgin A., EXPERIMENTAL EVALUATION OF MOMENTUM TERMS IN TURBULENT PIPE FLOW, NACA TN 3266, January, 1955.

22. Schlichting, Hermann G., Boundary Layer Theory, McGraw-Hill Book Publishing Company, Inc., New York, New York, 1960.

23. Van Driest, E. R., Journal of Applied Mechanics, 12, A91, 1945.

24. Welch, N. E. and Tomme, W. J., THE ANALYSIS OF TURBULENCE FROM DATA OBTAINED WITH A LASER VELOCIMETER, AIAA 67-179, 1967.

25. Winter, E. F. and Deterding J. H., British Journal of Applied Physics, 7,247, 1956.

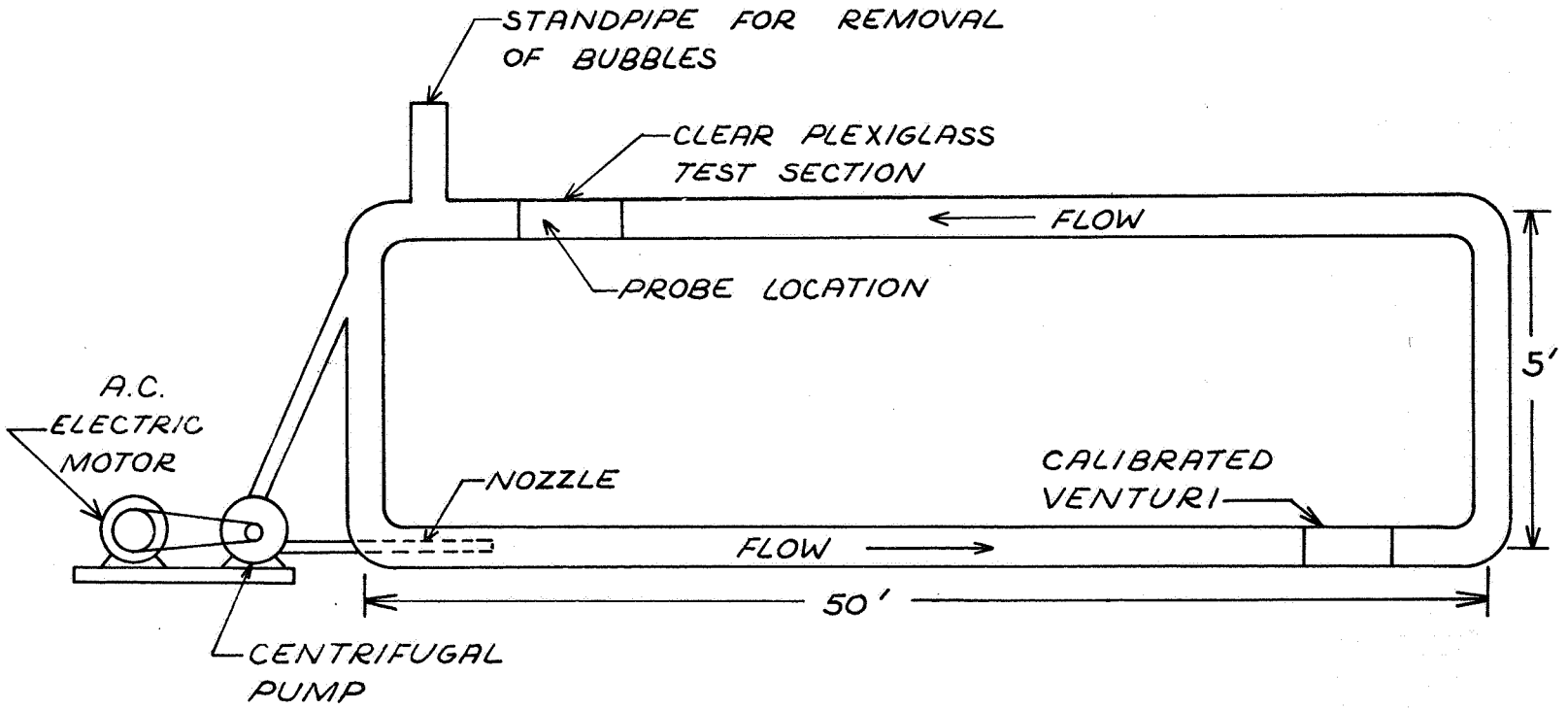

Figure 1. Schematic Diagram of Pipe Flow Facility.

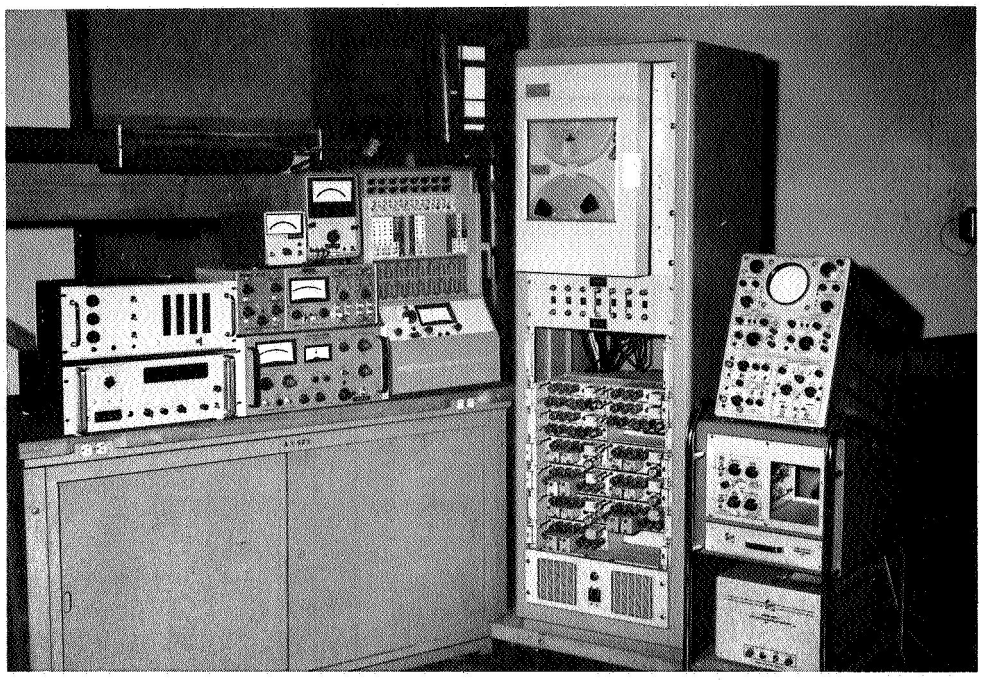

(a)

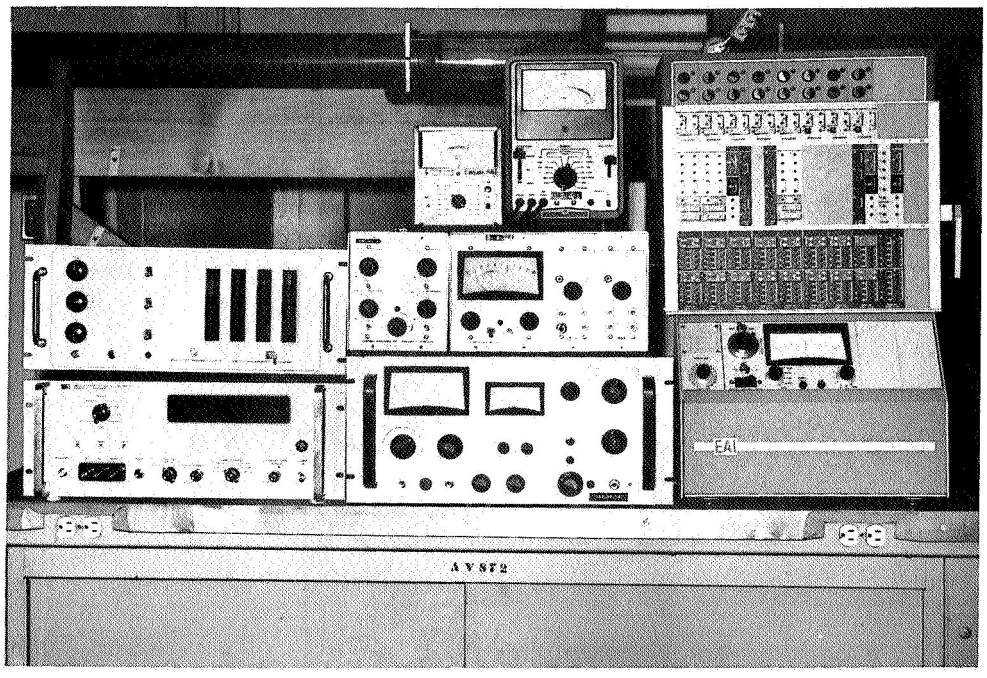

(b)

Figure 2. Hot-Film Anemometer and Recording Systems.

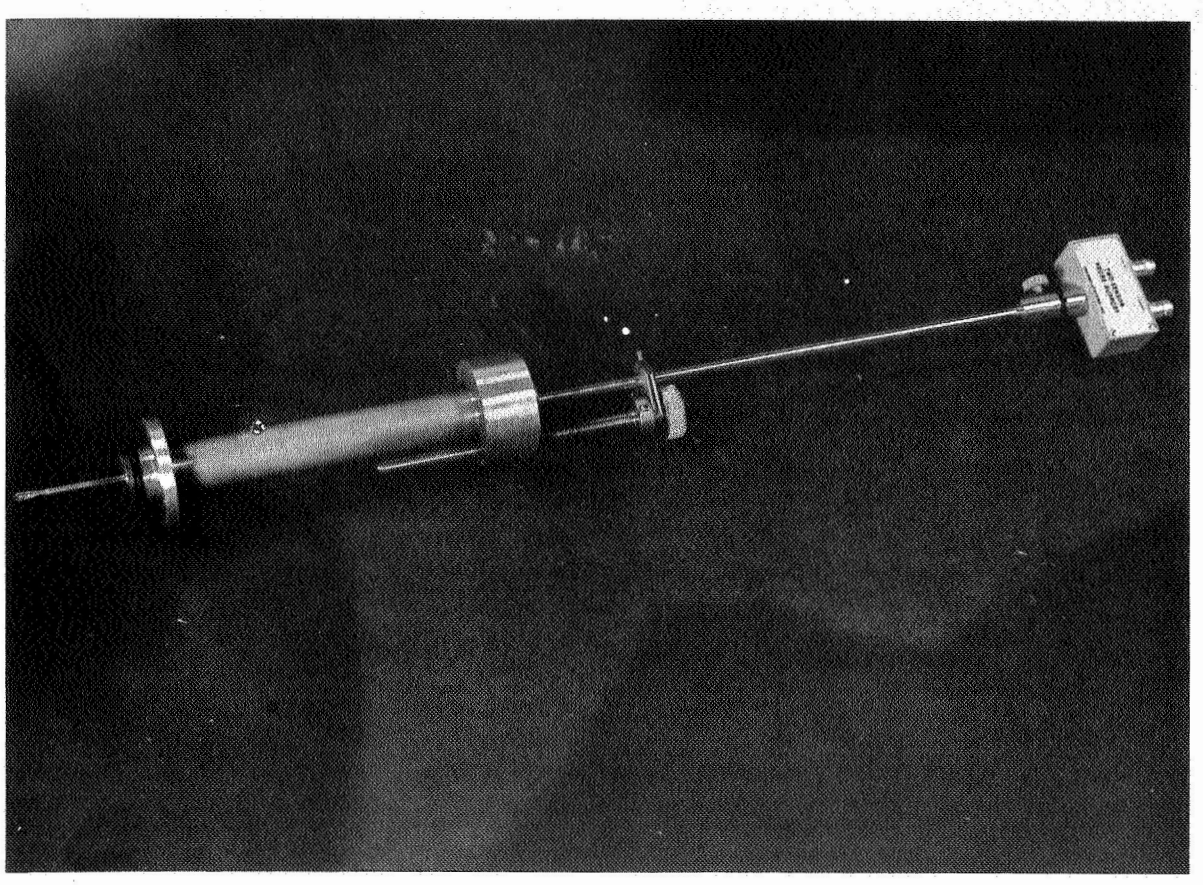

Figure 3. Hot-Film Anemometer Probe and Traversing Apparatus.

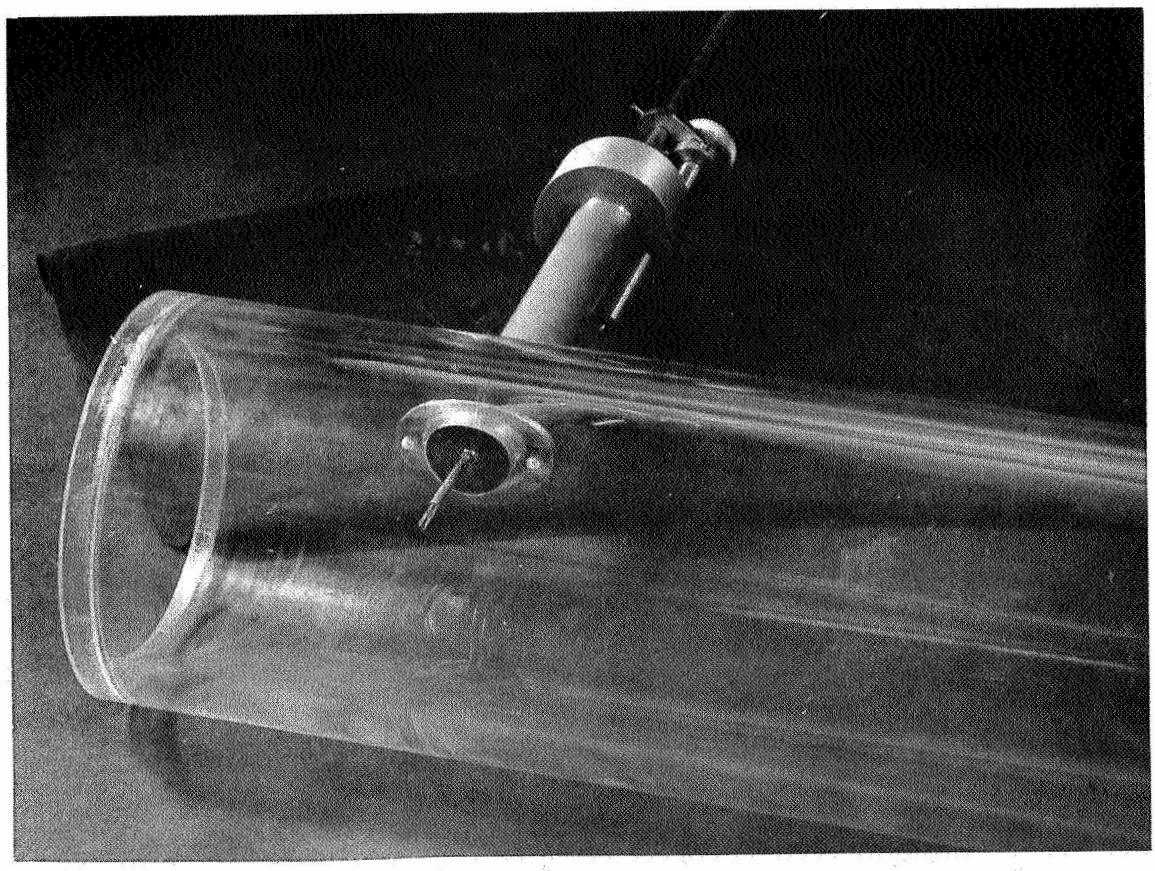

Figure 4. Hot-Film Probe Installed in Test Section.

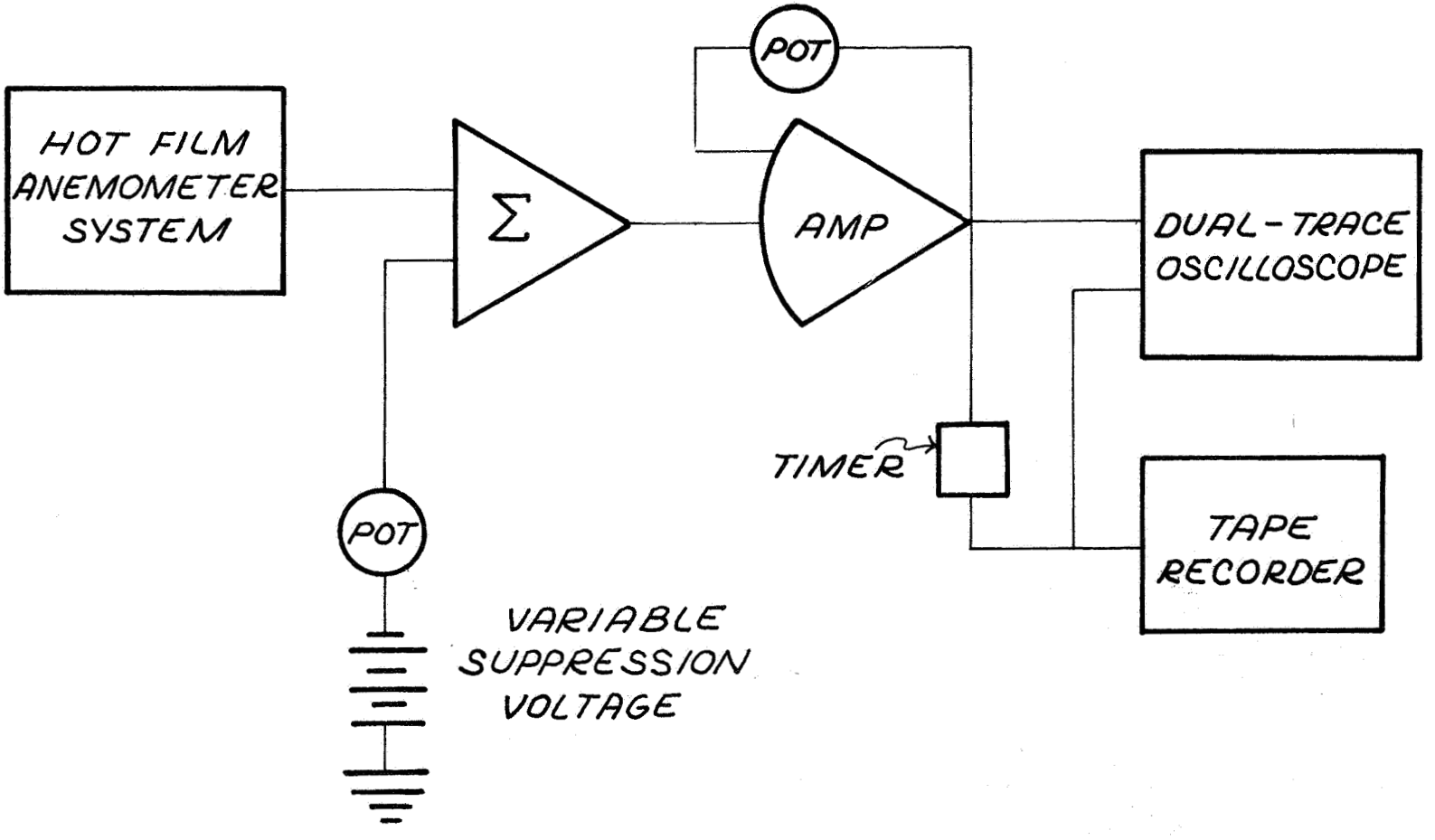

Figure 5. Schematic Diagram of Recording System.

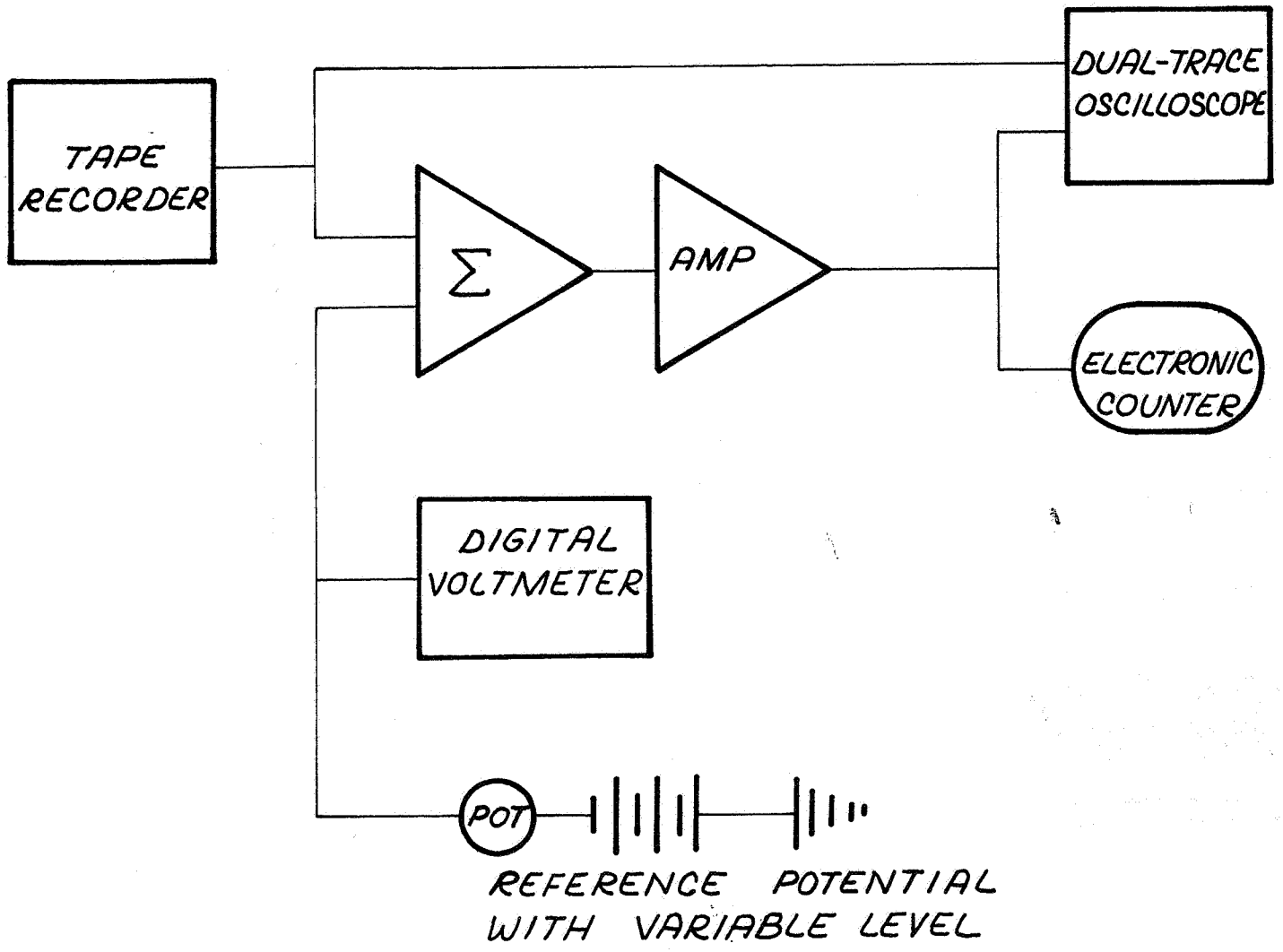

Figure 6. Schematic Diagram of Playback System.

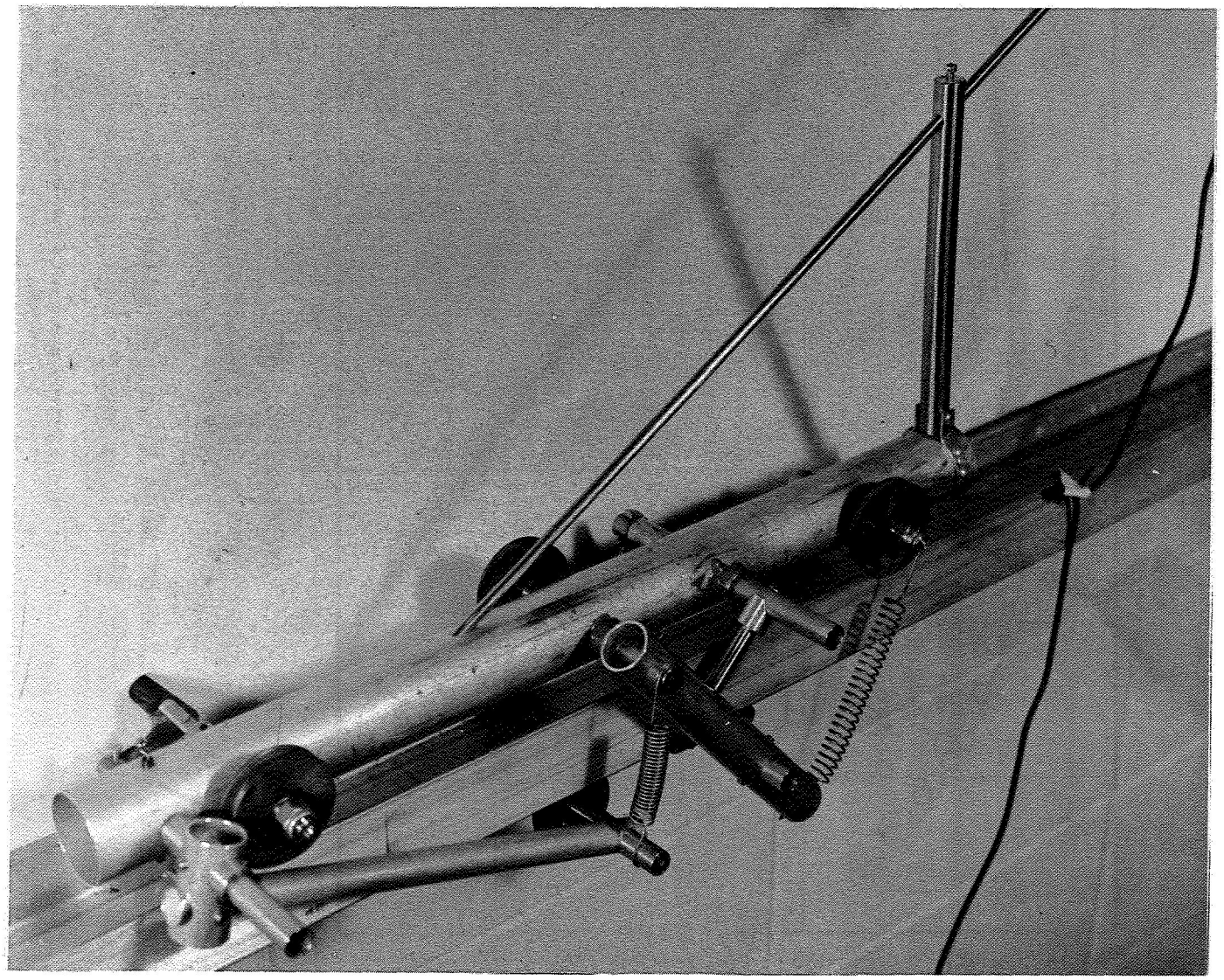

Figure 7. Calibration Cart and Channel.

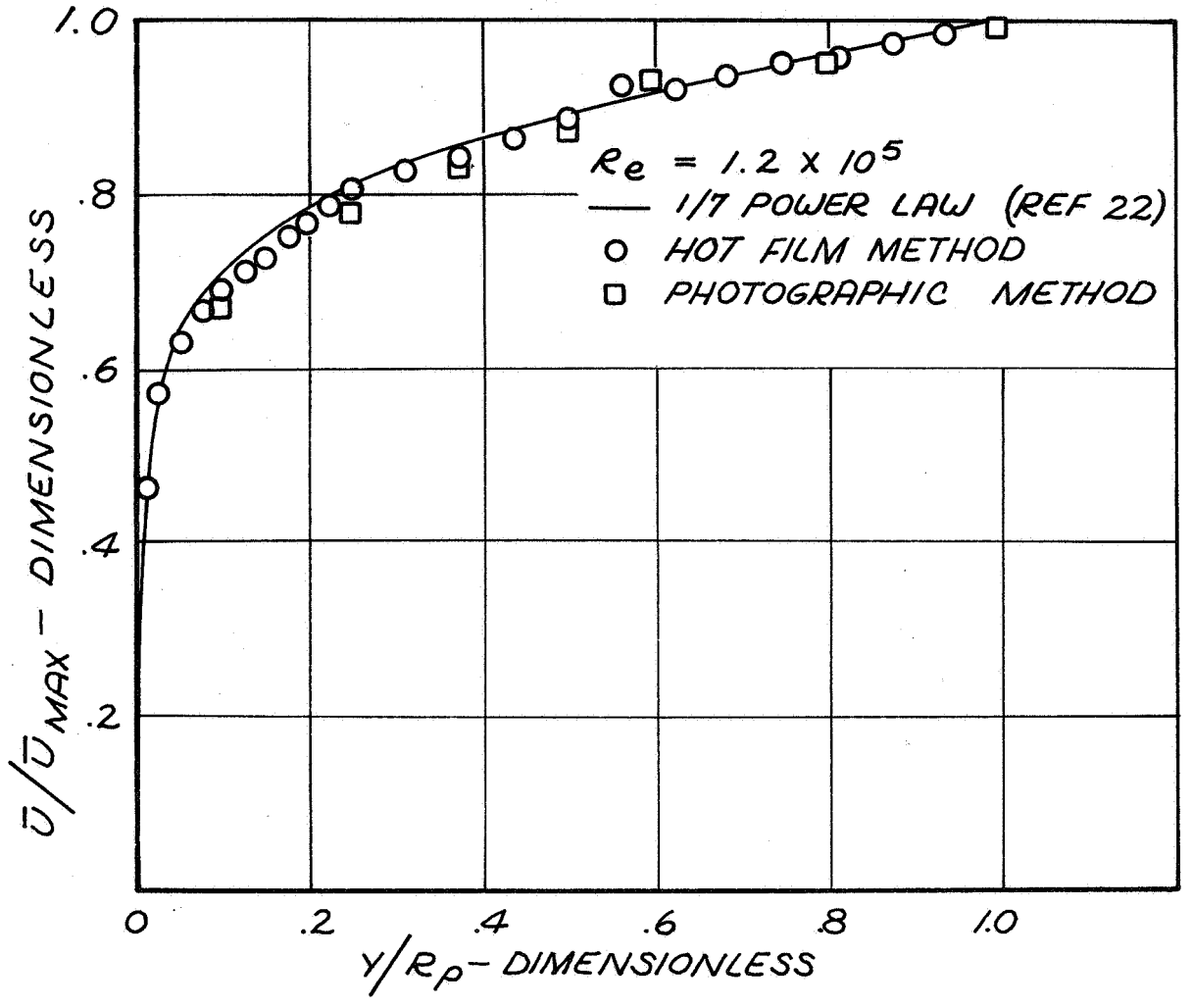

Figure 8. Variation of Mean Velocity With Distance From Pipe Wall.

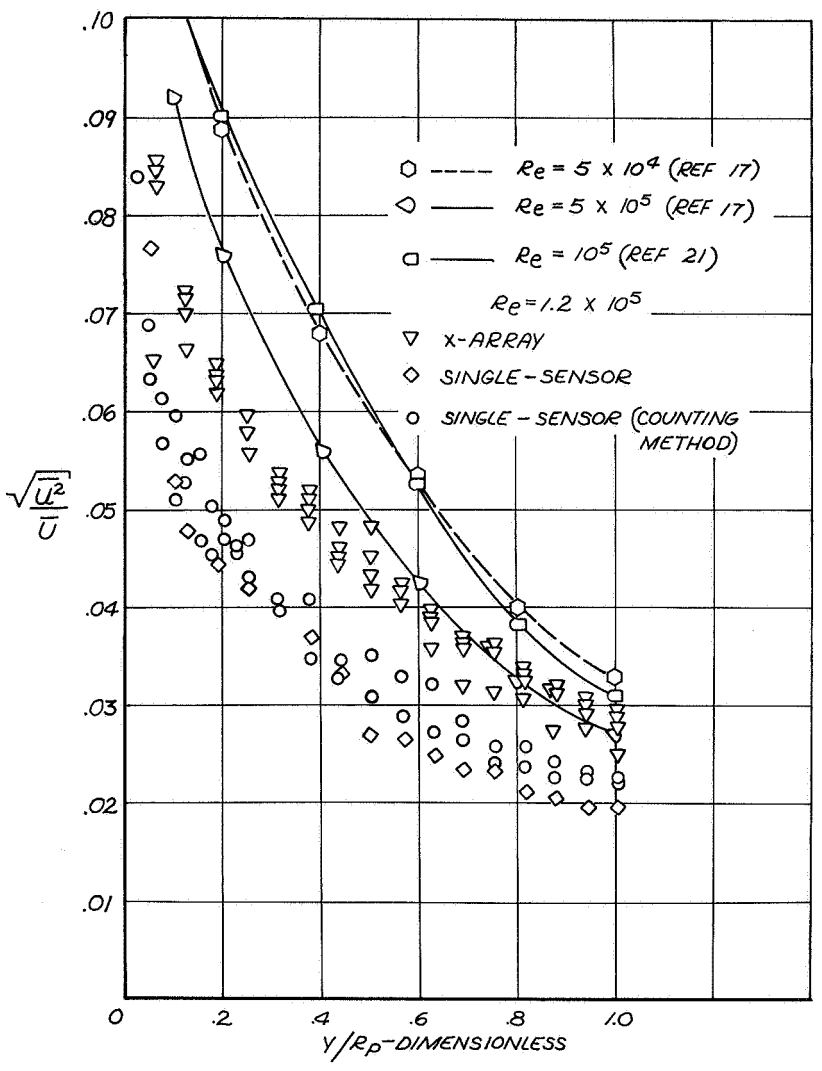

Figure 9. Variation of Axial Turbulence Intensity With Distance From Pipe Wall.

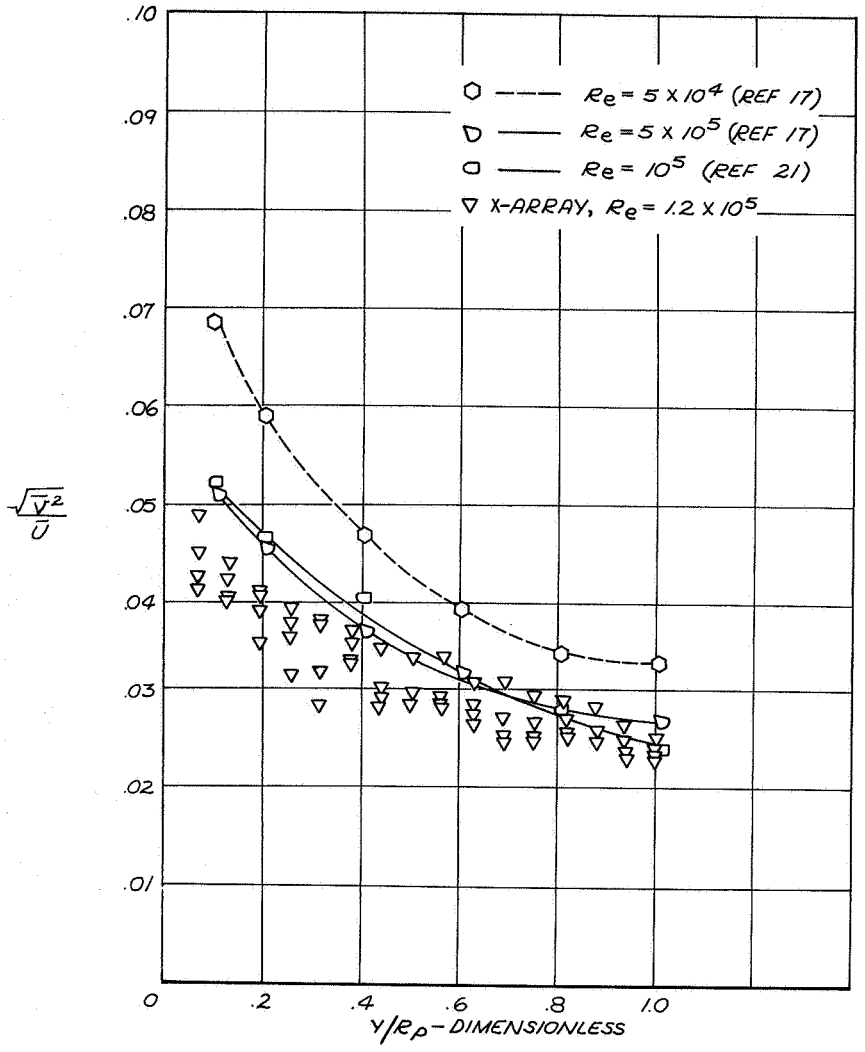

Figure 10. Variation of Radial Turbulence Intensity With Distance From Pipe Wall.

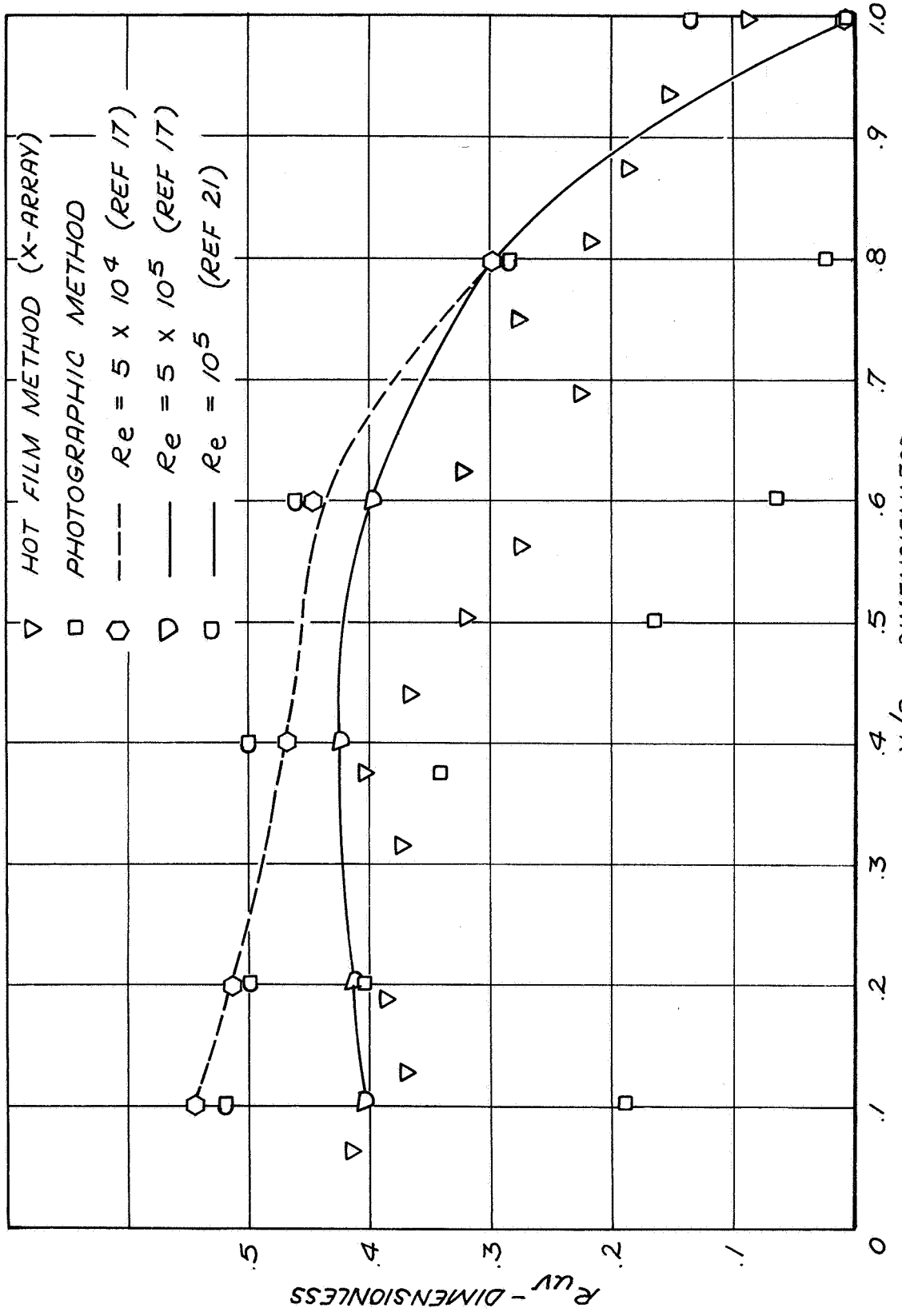

Figure 11. Variation of uv-Correlation Coefficient With Distance From Pipe Wall.

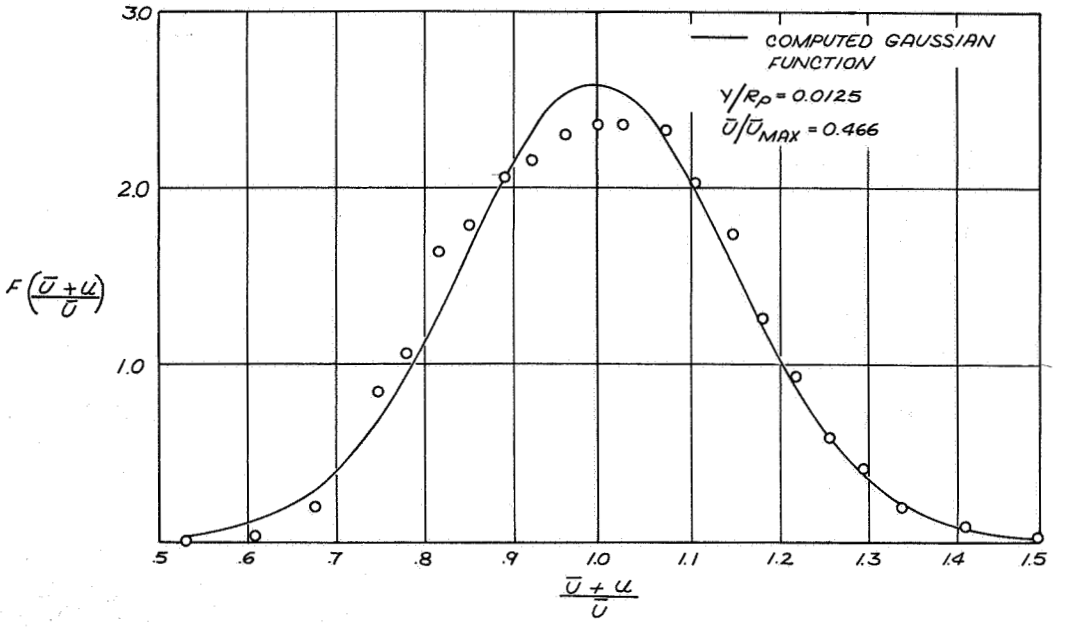

Figure 12a. Comparison of Distribution of Axial Velocity About Mean Velocity at $Y/R_p = 0.0125$ With Computed Gaussian Distribution.

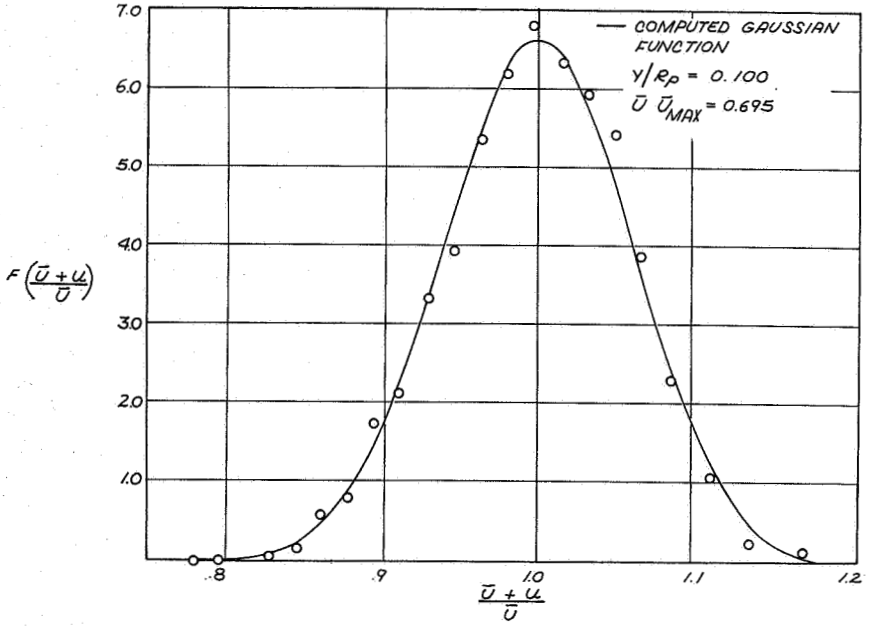

Figure 12b. Comparison of Distribution of Axial Velocity About Mean Velocity at $Y/R_p = 0.100$ With Computed Gaussian Distribution.

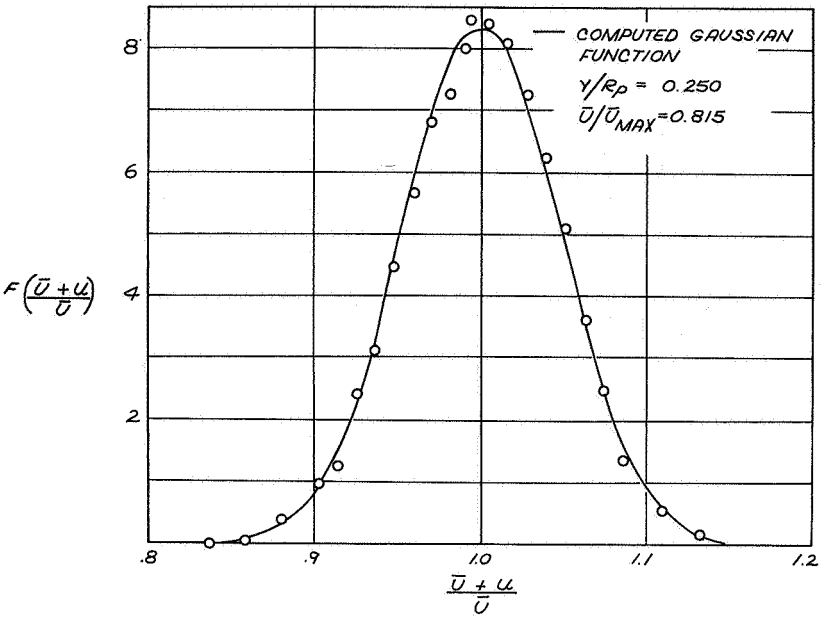

Figure 12c. Comparison of Distribution of Axial Velocity About Mean Velocity at $Y/R_p = 0.250$ With Computed Gaussian Distribution.

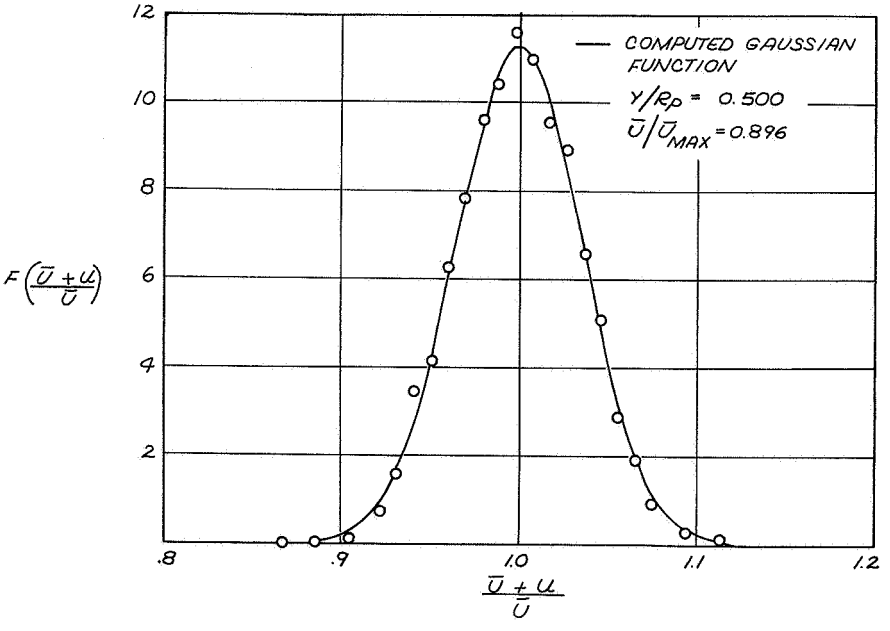

Figure 12d. Comparison of Distribution of Axial Velocity About Mean Velocity at $Y/R_p = 0.500$ With Computed Gaussian Distribution.

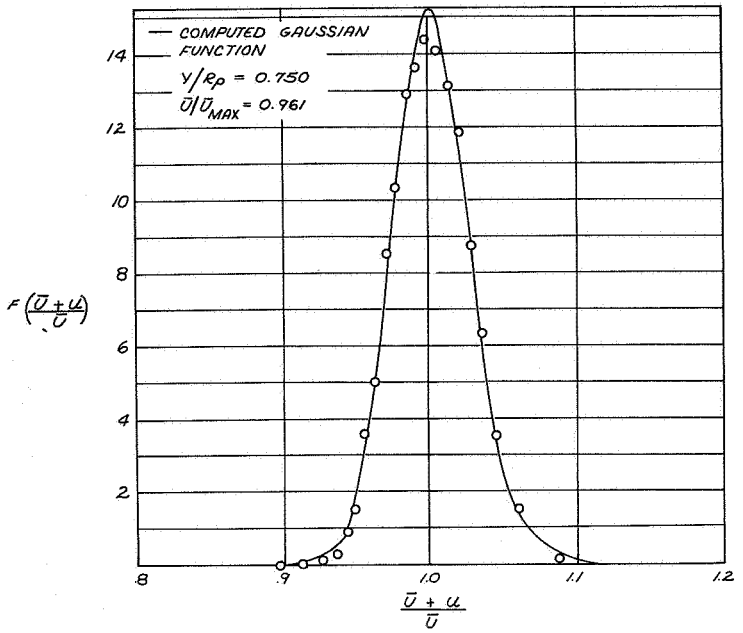

Figure 12e. Comparison of Distribution of Axial Velocity About Mean Velocity at $Y/R_p = 0.750$ With Computed Gaussian Distribution.

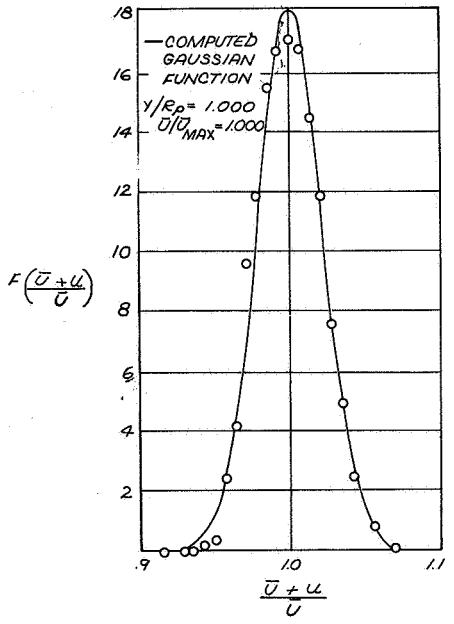

Figure 12f. Comparison of Distribution of Axial Velocity About Mean Velocity at $Y/R_p = 1.000$ With Computed Gaussian Distribution.

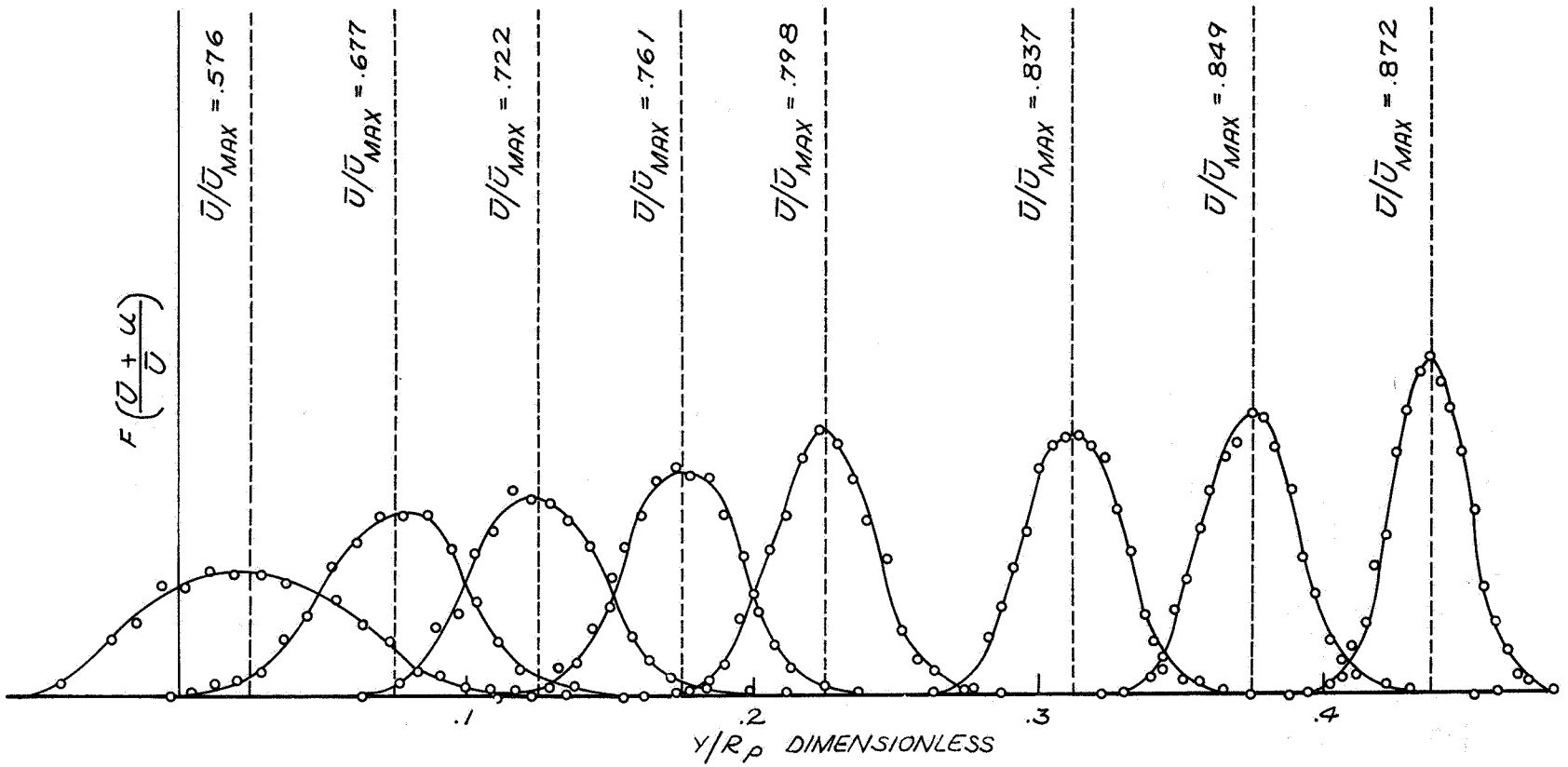

Figure 13. Variation of Velocity Distributions With Distance From Pipe Wall.

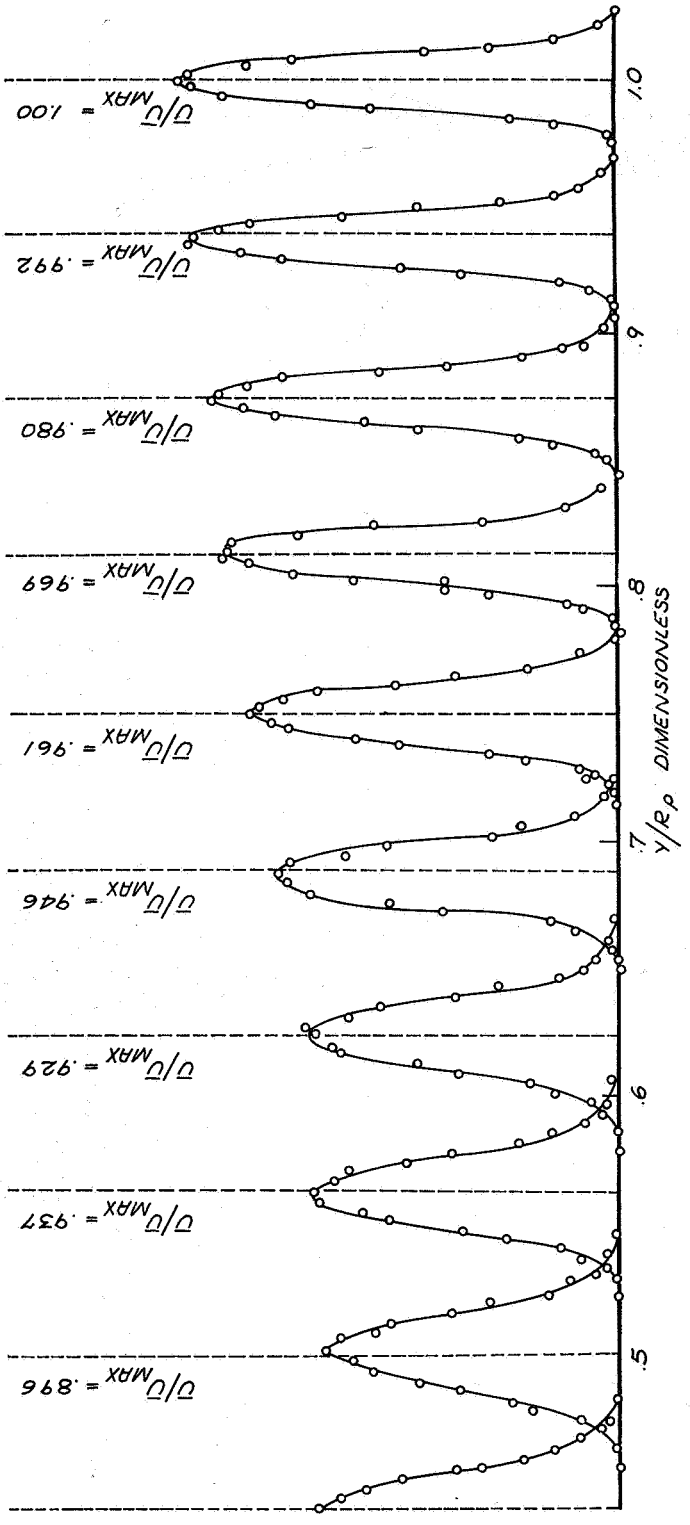

Figure 13.- Concluded

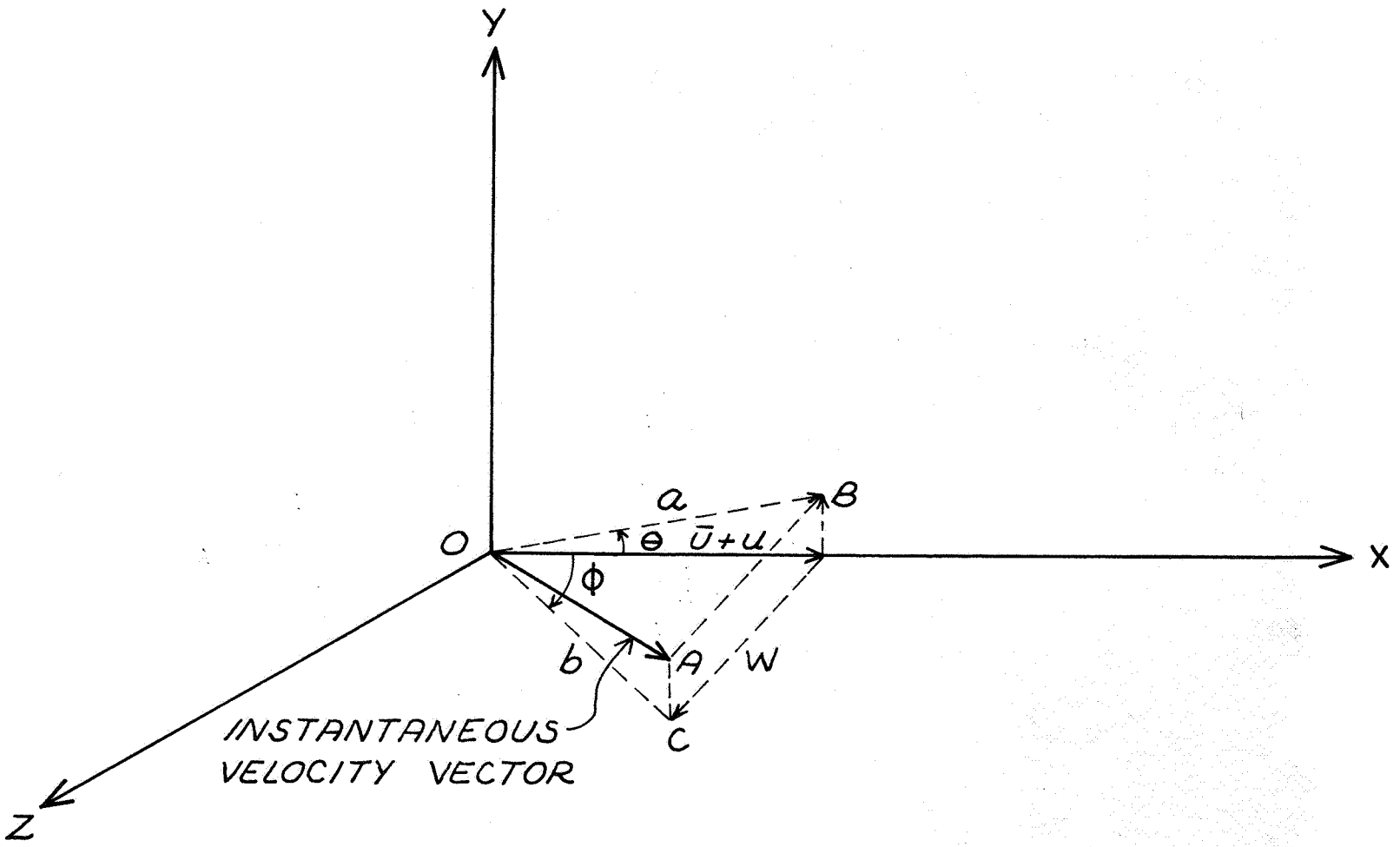

Figure 14. Coordinate System Used in Determining Velocity Fluctuations.

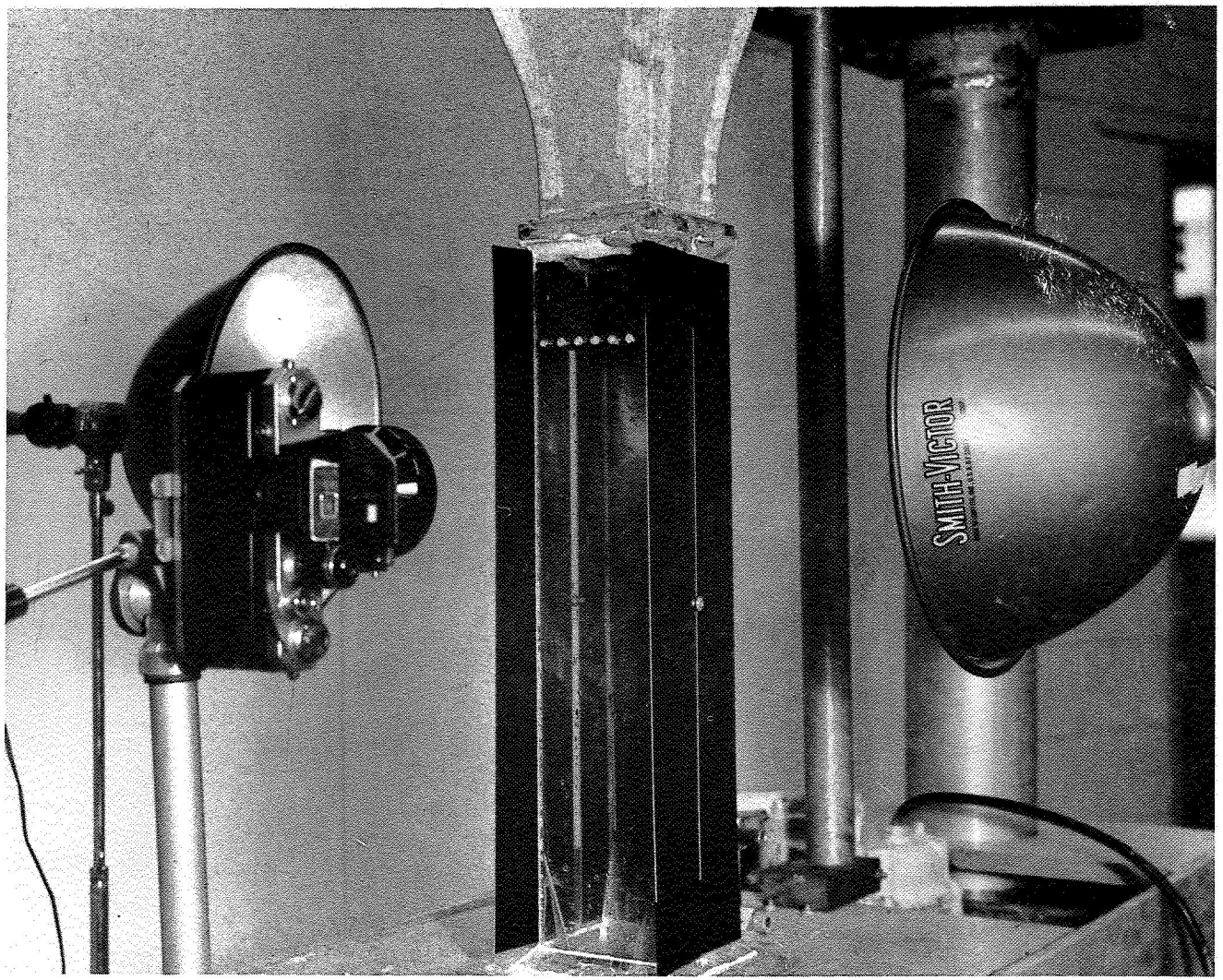

Figure 15. Experimental Arrangement Used in Flow Behind Parallel Bars.

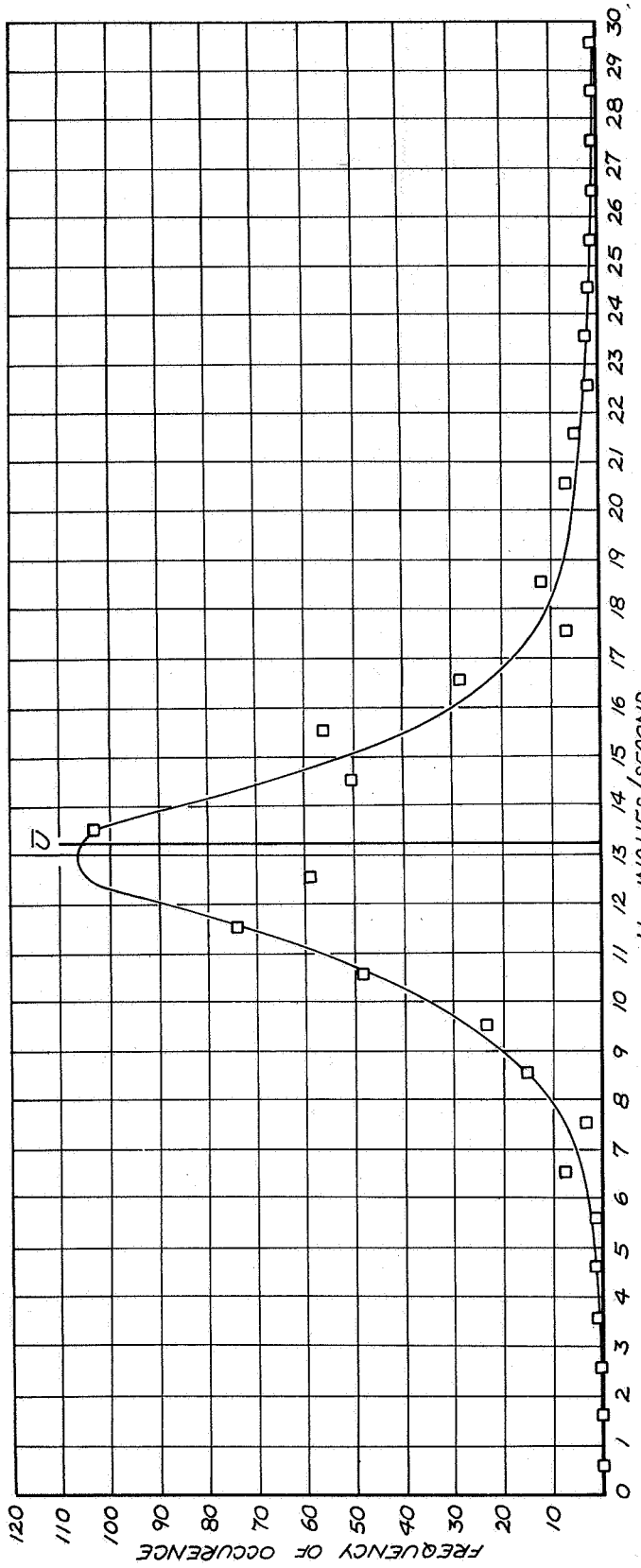

Figure 16. Frequency Distribution of U in Flow Behind Parallel Bars.

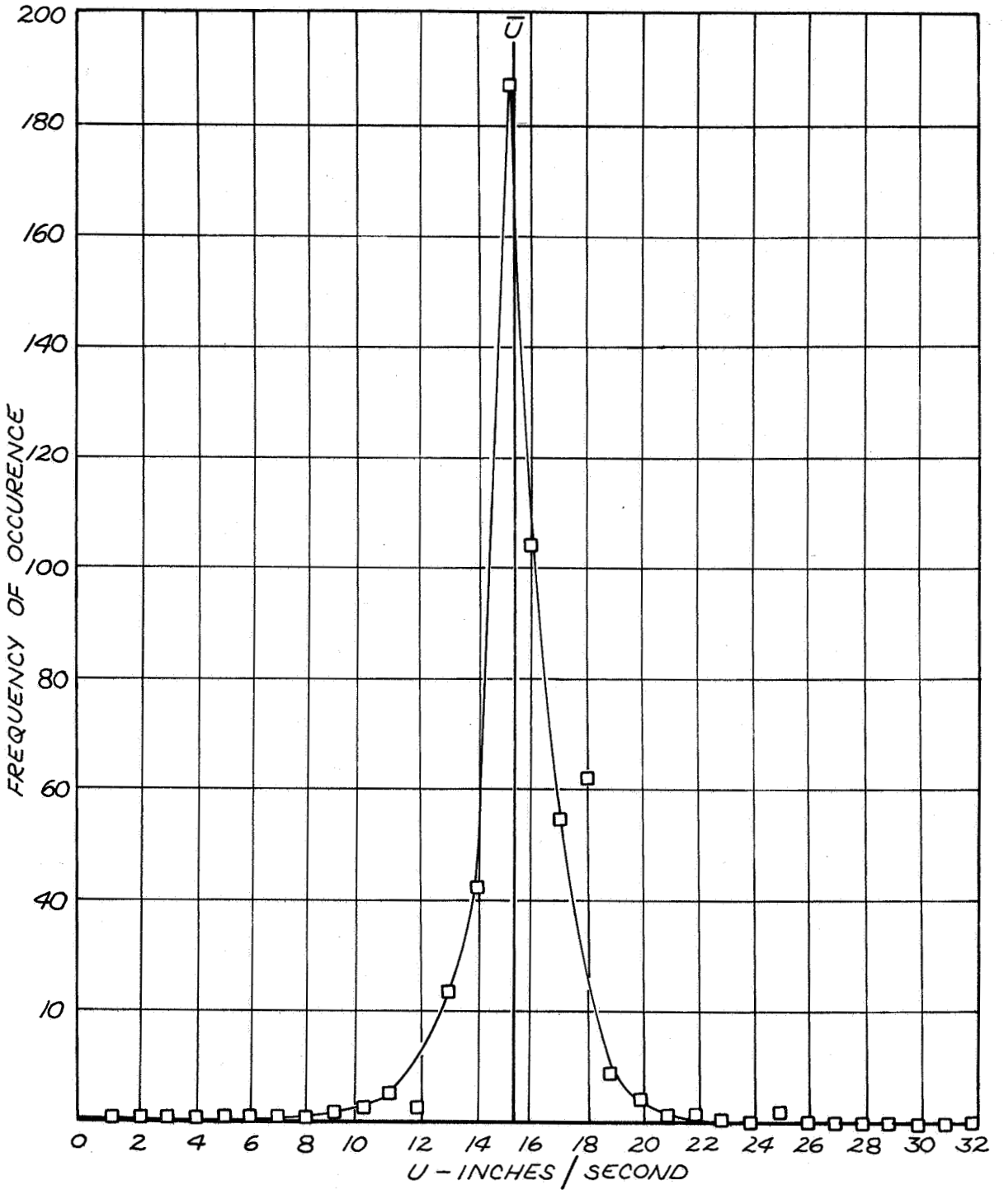

Figure 17. Frequency Distribution of U in Grid Flow.

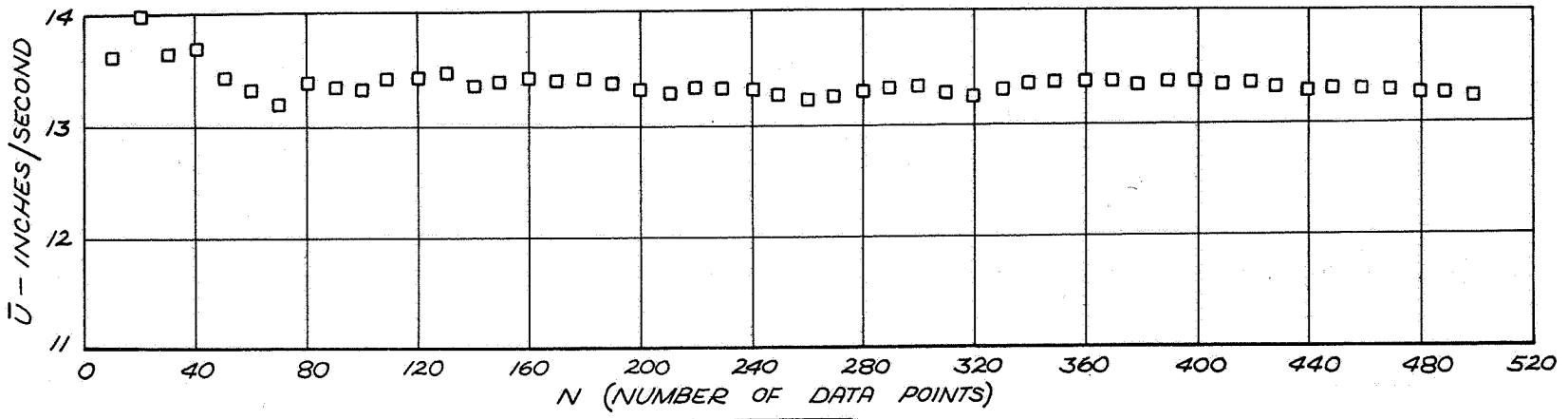

Figure 18a. Dependence of $\overline{U}$ on Number of Data Points Taken for Flow Behind Parallel Bars.

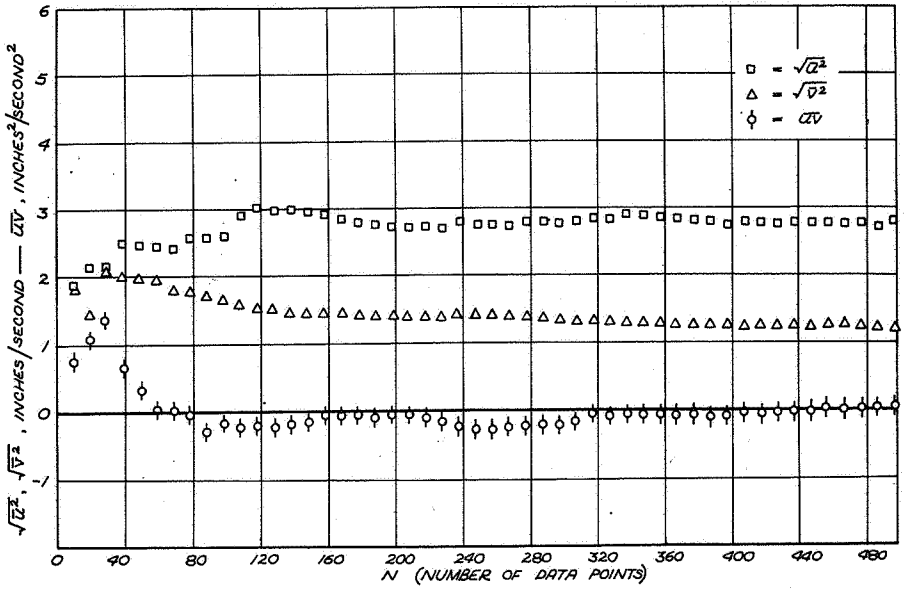

Figure 18b. Dependence of $\sqrt{\overline{u^2}}$, $\sqrt{\overline{v^2}}$, and $\overline{uv}$ on Number of Data Points Taken for Flow Behind Parallel Bars.

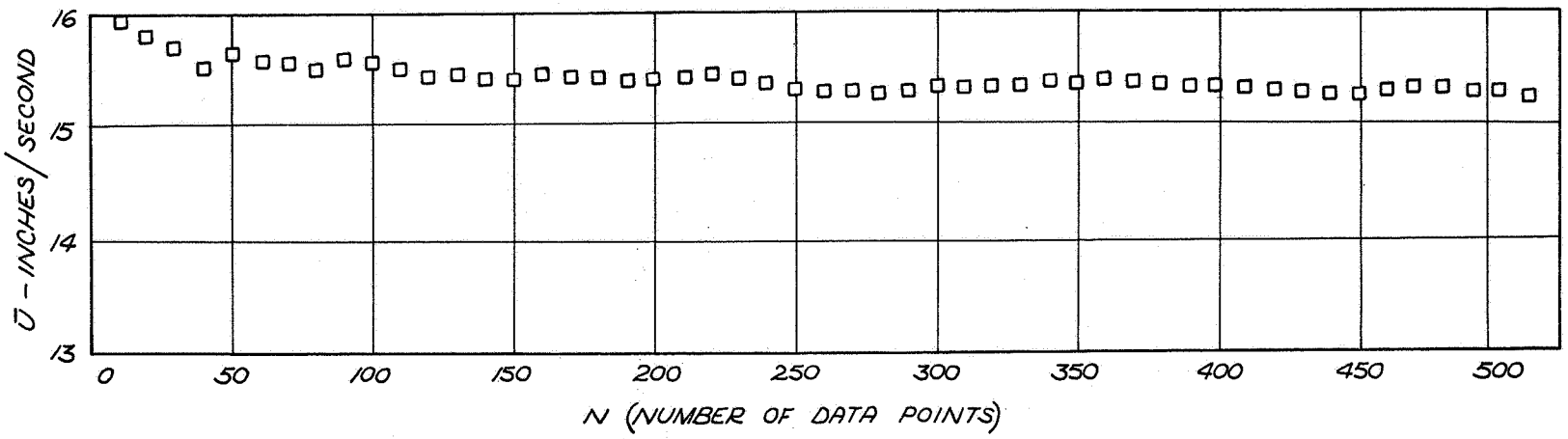

Figure 19a. Dependence of $\overline{U}$ on Number of Data Points Taken for Grid Flow.

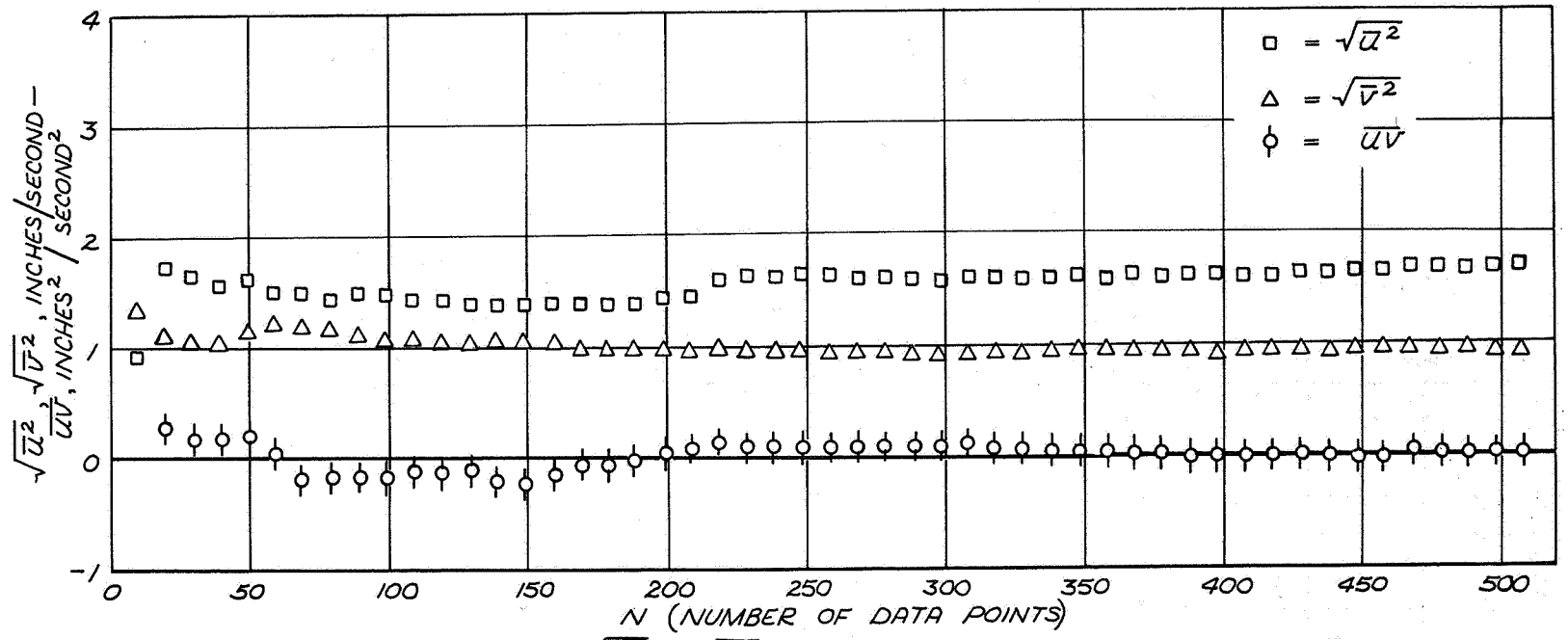

Figure 19b. Dependence of $\sqrt{\overline{u^2}}$, $\sqrt{\overline{v^2}}$, and $\overline{uv}$ on Number of Data Points Taken for Grid Flow.

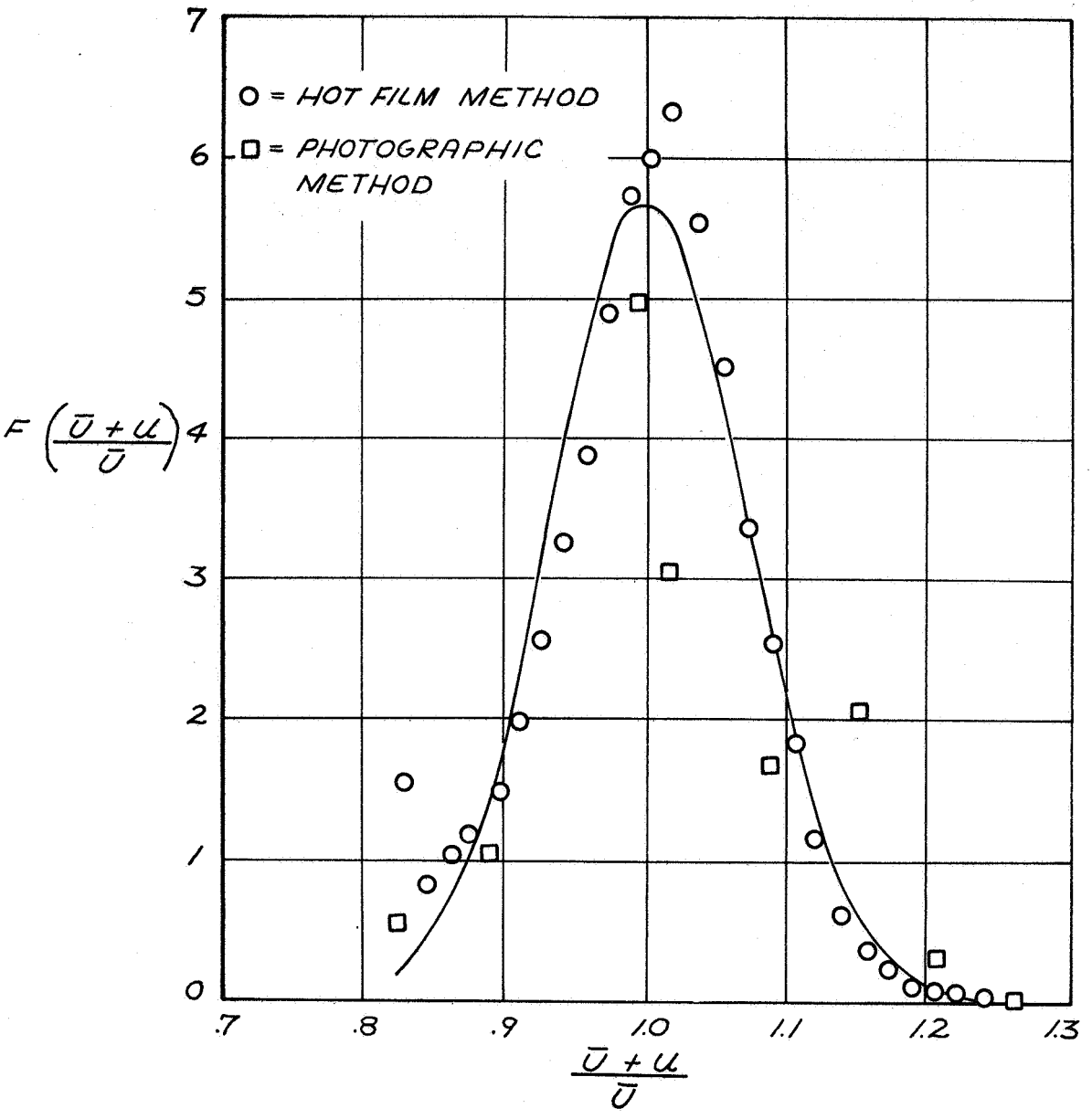

Figure 20. Frequency Distributions Obtained in Grid Flow by Photographic Method and by Hot-Wire Anemometer.

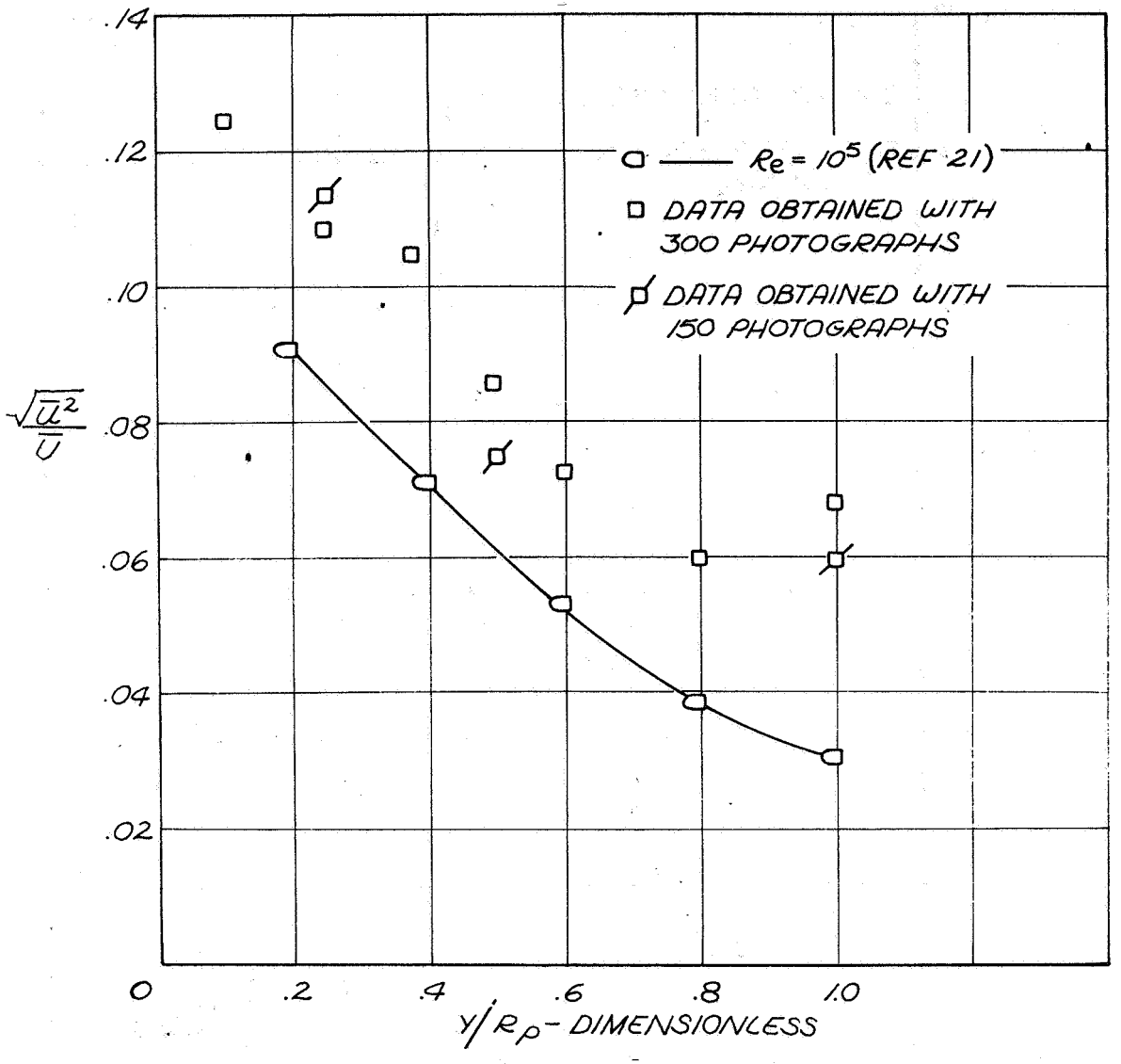

Figure 21. Variation of Axial Turbulence Intensity With Distance From Wall by Photographic Method.

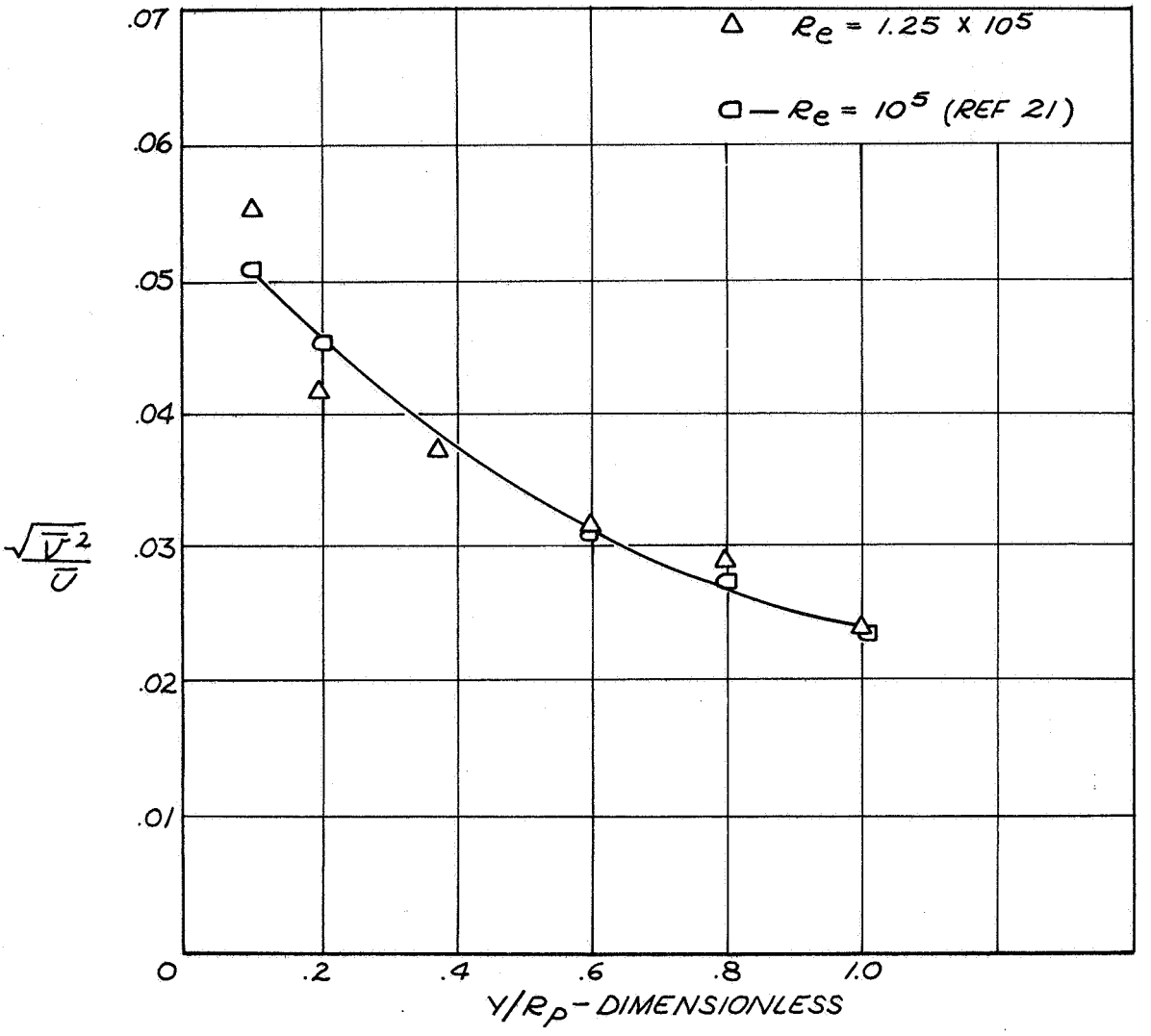

Figure 22. Variation of Radial Turbulence Intensity With Distance From Wall by Photographic Method.

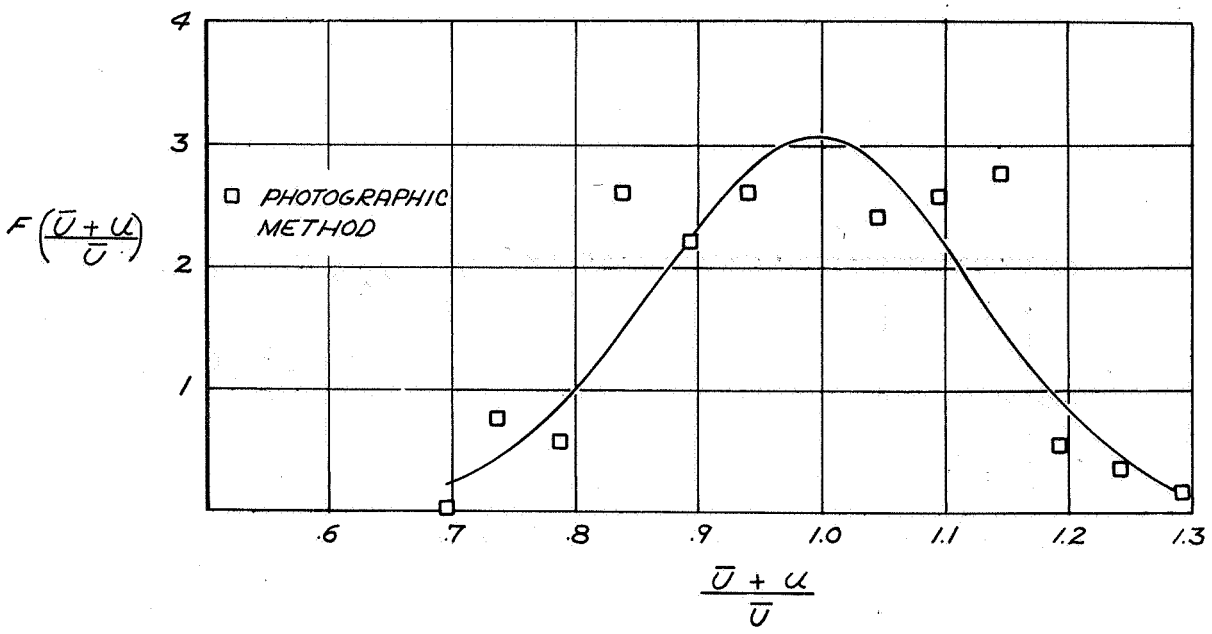

Figure 23a. Comparison of Measured Velocity Distribution in Pipe Flow Obtained by Photographic Method With Gaussian Distribution at $Y/R_p = 0.25$.

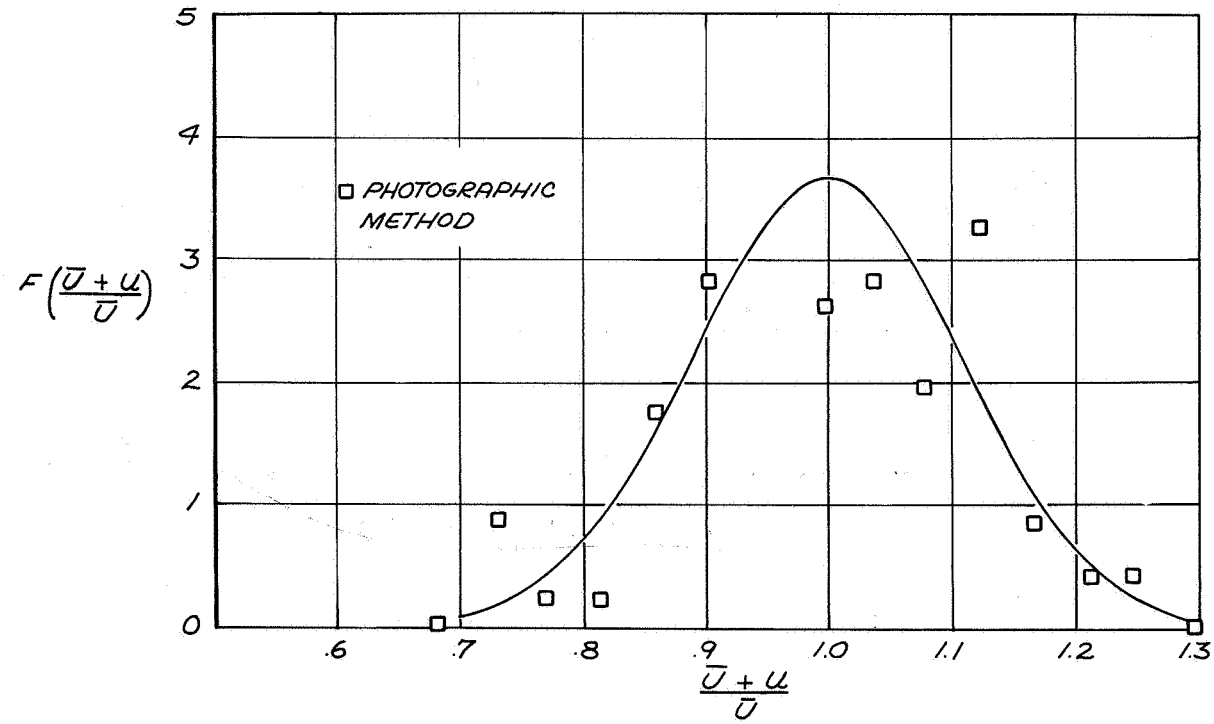

Figure 23b. Comparison of Measured Velocity Distribution in Pipe Flow Obtained by Photographic Method With Gaussian Distribution at $Y/R_p = 0.10$.